PALEOCEANOGRAPHY, VOL. 23, PA1203, doi:10.1029/2007PA001445, 2008

Meridional reorganizations of marine and terrestrial productivity during Heinrich events

L. Menviel,[1] A. Timmermann,[2] A. Mouchet,[3] and O. Timm[2]

Received 23 February 2007; revised 20 June 2007; accepted 20 September 2007; published 18 January 2008.

[1] To study the response of the global carbon cycle to a weakening of the Atlantic Meridional Overturning Circulation (AMOC), a series of freshwater perturbation experiments is conducted both under preindustrial and glacial conditions using the earth system model of intermediate complexity LOVECLIM. A shutdown of the AMOC leads to substantial cooling of the North Atlantic, a weak warming of the Southern Hemisphere, intensification of the northeasterly trade winds, and a southward shift of the Intertropical Convergence Zone (ITCZ). Trade wind anomalies change upwelling in the tropical oceans and hence marine productivity. Furthermore, hydrological changes associated with a southward displacement of the ITCZ lead to a reduction of terrestrial carbon stocks mainly in northern Africa and northern South America in agreement with paleoproxy data. In the freshwater perturbation experiments the ocean acts as a sink of CO_2, primarily through increased solubility. The net atmospheric CO_2 anomaly induced by a shutdown of the AMOC amounts to about +15 ppmv and −10 ppmv for preindustrial and glacial conditions, respectively. This background state dependence can be explained by the fact that the glacial climate is drier and the terrestrial vegetation therefore releases a smaller amount of carbon to the atmosphere. This study demonstrates that the net CO_2 response to large-scale ocean circulation changes has significant contributions both from the terrestrial and marine carbon cycle.

Citation: Menviel, L., A. Timmermann, A. Mouchet, and O. Timm (2008), Meridional reorganizations of marine and terrestrial productivity during Heinrich events, *Paleoceanography*, *23*, PA1203, doi:10.1029/2007PA001445.

1. Introduction

[2] Paleoproxys clearly document [*Vidal et al.*, 1997; *McManus et al.*, 2004] that Heinrich events, interpreted as manifestations of major glacial ice sheet instabilities [*Heinrich*, 1988], weakened the Atlantic overturning circulation with impacts on the large-scale climate system. Ice cores from Greenland [*Dansgaard et al.*, 1993], marine sediment cores from the North Atlantic [*Bond et al.*, 1992; *Bond*, 1993], the North Pacific [*Harada et al.*, 2006] and the Mediterranean Sea [*Rohling et al.*, 1998; *Cacho et al.*, 1999] as well as lake and loess records from Europe [*Shi et al.*, 2003; *Watts et al.*, 1996; *Thouveny et al.*, 1994] and Asia [*Swann et al.*, 2005] provide unequivocal evidence for a widespread Northern Hemispheric cooling during Heinrich events, prevailing for several hundreds to thousand of years. Similar climate anomalies occurred in response to a slow down of the Atlantic Meridional Overturning Circulation (AMOC) [*McManus et al.*, 2004] during the Younger Dryas (YD) cold interval around 12.7–11.6 ka B.P. Unlike the Heinrich events that were associated with iceberg surges throughout the North Atlantic, the YD event has been linked to the drainage of Lake Agassiz [*Teller et al.*, 2002; *Carlson et al.*, 2007], which added significant freshwater into the North Atlantic [*Fairbanks*, 1989]. Although their triggers were substantially different, it is conceivable to assume that Heinrich events and the YD exhibited similar climate-carbon cycle responses.

[3] The interhemispheric response pattern of Heinrich events has been successfully reconstructed using high-resolution Antarctic ice cores that were synchronized to well-dated Greenland ice cores via methane concentrations [*Blunier and Brook*, 2001]. The results support the notion of a bipolar seesaw [*Broecker*, 1998; *Stocker*, 1998] which is characterized to first order by an out-of-phase relationship between northern and Southern Hemispheric temperatures. Only recently have modeling studies elucidated the physical mechanisms that are responsible for spreading the northern North Atlantic cooling equatorward [*Stouffer et al.*, 2006; *Timmermann et al.*, 2007; *Krebs and Timmermann*, 2007] and for warming the Southern Hemisphere. While the equatorward spreading of the North Atlantic sea surface temperature (SST) anomaly involves air-sea coupling via the wind-evaporation SST (WES) feedback, the South Atlantic warming can be mostly explained in terms of reduced meridional oceanic heat transports. Heinrich anomalies were also associated with global sea level anomalies in the order of 3–30 m [*Siddall et al.*, 2003; *Lambeck et al.*, 2002].

[4] Most recent modeling studies of Heinrich events have focused on the large-scale physical effects. However, little is known about the global carbon cycle response to a weakened AMOC. Synthesizing existing proxy evidence of

[1]Department of Oceanography, University of Hawai'i at Manoa, Honolulu, Hawaii, USA.
[2]International Pacific Research Center, School of Ocean and Earth Science and Technology, University of Hawai'i at Manoa, Honolulu, Hawaii, USA.
[3]Département Astrophysique, Géophysique et Océanographie, Université de Liège, Liège, Belgium.

0883-8305/08/2007PA001445$12.00

marine and terrestrial productivity changes during Heinrich events has been hampered by the sparseness of these records and the lack of suitable model simulations. Furthermore understanding the apparent linkage between glacial CO_2 changes [*Monnin et al.*, 2001; *Stauffer et al.*, 1998; *Indermühle et al.*, 1999] and Heinrich events has been a major challenge because the relative phasing among the two is still difficult to establish. Possible linkages between millennial-scale CO_2 changes and Heinrich events were identified and elucidated using two-dimensional ocean-energy balance marine carbon cycle models [*Marchal et al.*, 1998, 1999] and vegetation models, such as the Lund-Potsdam Jena Dynamic Global Vegetation Model (LPJ-DGVM). Neglecting vegetation effects *Marchal et al.* [1998, 1999] found a 10–30 ppmv CO_2 change in response to an AMOC shutdown. This response was explained in terms of reduced ocean solubility, due to enhanced southern ocean temperatures. On the other hand, employing only a crude marine carbon cycle component but a complex vegetation model *Scholze et al.* [2003b] and *Köhler et al.* [2005] identified the Northern Hemispheric vegetation as an important source for CO_2 during periods of reduced AMOC.

[5] It is timely to revisit the issue of millennial-scale carbon cycle dynamics using a model that captures both, the terrestrial and the marine carbon cycle adequately and that can be run for many centuries. The goal of our study is to quantify the relative contributions of these two components to the CO_2 sensitivity under millennial-timescale freshwater forcing, both under present-day and glacial conditions.

2. Earth System Model LOVECLIM

[6] The atmospheric component of the coupled atmosphere-ocean–sea ice–carbon cycle model LOVECLIM is ECBilt [*Opsteegh et al.*, 1998], a spectral T21, three-level model, based on quasi-geostrophic equations extended by estimates of the neglected ageostrophic terms [*Lim et al.*, 1991] in order to close the equations at the equator. The model contains a full hydrological cycle which is closed over land by a bucket model for soil moisture. Synoptic variability associated with weather patterns is explicitly computed. Diabatic heating due to radiative fluxes, the release of latent heat and the exchange of sensible heat with the surface are parameterized. Compared to the standard version of LOVECLIM we enhanced the sensitivity of ECBilt to longwave radiation forcing by a factor of 2 [*Timm and Timmermann*, 2007]. The simulated global mean temperature response to such a perturbation amounts to about 3°C as compared to the 1.5°C for the standard sensitivity. The qualitative structure of the climate change pattern is stable to reasonable changes in the longwave sensitivity. For our simulations, the time-varying daily averaged incoming insolation is calculated as a function of latitude using the algorithm of *Berger* [1978].

[7] The sea ice–ocean component of LOVECLIM, CLIO [*Goosse et al.*, 1999; *Goosse and Fichefet*, 1999; *Campin and Goosse*, 1999] consists of a free-surface primitive equation model with $3° \times 3°$ resolution coupled to a thermodynamic-dynamic sea ice model. Coupling between atmosphere and ocean is done via the exchange of freshwater and heat fluxes, rather than by virtual salt fluxes. To avoid a singularity at the North Pole, the oceanic component makes use of two subgrids: The first one is based on classic longitude and latitude coordinates and covers the whole ocean, except for the North Atlantic and Arctic Ocean. These are covered by the second spherical subgrid, which is rotated and has its poles at the equator in the Pacific (111°W) and Indian Ocean (69°E).

[8] The terrestrial vegetation module of LOVECLIM, VECODE, described by *Brovkin et al.* [1997], has recently been coupled to the LOVECLIM model [*Renssen et al.*, 2005]. On the basis of annual mean values of several climatic variables, the VECODE model computes the evolution of the vegetation cover described as a fractional distribution of desert, tree, and grass in each land grid cell once a year. To better compare the results, we developed a module to assign biomes based on VECODE and ECBilt outputs. This module is equivalent to the one described by *Roche et al.* [2006], except that we grouped the temperate broadleaf forest and the cool mixed forest into a biome called mixed forest. Within the LOVECLIM version used here, simulated vegetation changes affect only the land surface albedo, and have no influence on other processes such as evapotranspiration.

[9] LOCH is a three-dimensional global model of the oceanic carbon cycle with prognostic equations for dissolved inorganic carbon (DIC), total alkalinity, phosphates (PO_4^{3-}), organic products, oxygen and silicates [*Mouchet and Francois*, 1996; *Fichefet et al.*, 2006]. LOCH is fully coupled to CLIO, using the same time step. In addition to their biogeochemical transformations, tracers in LOCH are advected with the CLIO circulation field and experience horizontal and vertical mixing. The near-surface oceanic uptake of CO_2 is governed by the solubility as well as the regional biological processes. The partial pressure of CO_2 in the surface waters is calculated from the total alkalinity and DIC tracers. The difference between the partial pressure of CO_2 in the ocean and in the atmosphere, modulated by a wind-dependent exchange coefficient, determines the net CO_2 air-sea fluxes. LOCH computes the export production from the state of a phytoplankton pool in the euphotic zone (0–120 m). The phytoplankton growth depends on the availability of nutrients (PO_4^{3-}) and light, with a weak temperature dependence. A grazing process together with natural mortality limit the primary producers biomass and provide the source term for the organic matter sinking to depth. Remineralization of organic matter depends on oxygen availability, but anoxic remineralization can also occur. Depending on the silica availability, phytoplankton growth is accompanied by the formation of opal or $CaCO_3$ (calcite and aragonite) shells, which then sink to depth. $CaCO_3$ shells are dissolved depending on the calcite and aragonite saturation states, whereas a simple constant rate is used for opal. The organic matter that is not remineralized and the shells that are not dissolved are permanently preserved in the sediments. This leads to a loss of alkalinity, carbon, phosphates and silicates, which is compensated by the river influx of these components. The atmospheric CO_2 content is predicted for each ocean time step from the air-

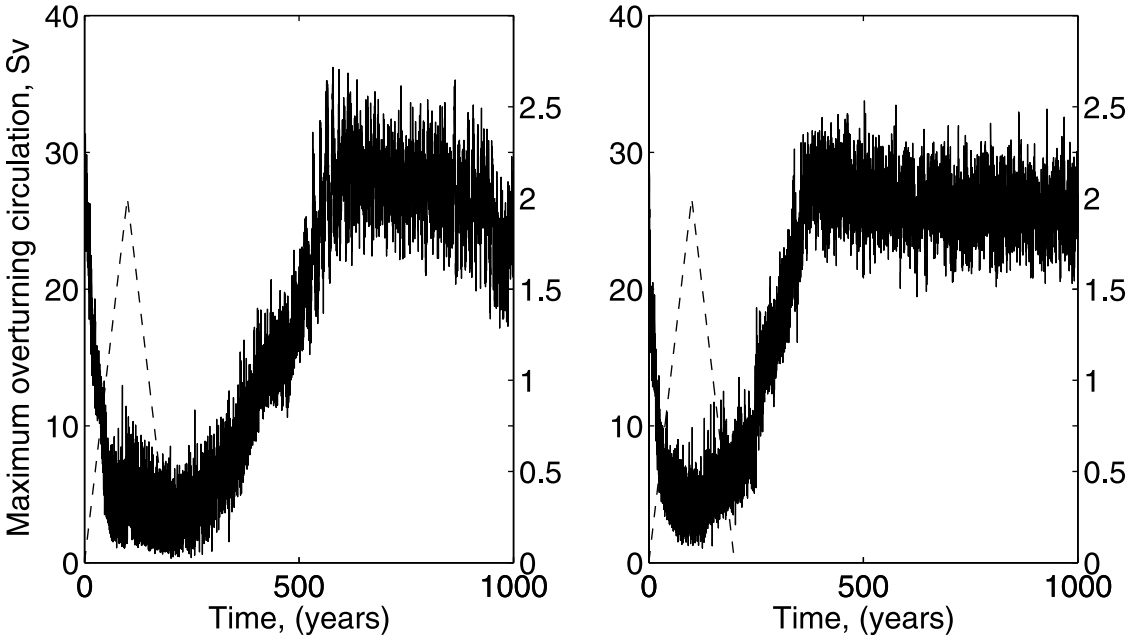

Figure 1. Maximum of the meridional stream function (sverdrup (Sv) 1 Sv = 10^6 m^3 s^{-1}) in the North Atlantic (solid line) for (left) FC and (right) FL. Anomalous freshwater flux (Sv) into the northern North Atlantic (dashed line) for (left) FC and (right) FL is shown.

sea CO_2 fluxes calculated by LOCH as well as from the air-terrestrial biomass CO_2 fluxes provided by VECODE.

3. Experimental Setup and Model Performance

3.1. Preindustrial and Last Glacial Maximum Control Simulations

[10] The preindustrial steady state (PIN) was obtained by forcing LOVECLIM with 278 ppmv of atmospheric CO_2 during 500 years, then allowing the atmospheric CO_2 to vary freely during 700 years.

[11] To obtain a quasi-equilibrium state for Last Glacial Maximum (LGM) conditions (simulation LGM), ECBilt-CLIO-LOCH were forced for 2200 years using LGM orbital parameters, the glacial topography [*Peltier*, 1994], the associated albedo pattern, LGM forest fraction [*Crowley and Baum*, 1997] as well as with the LGM atmospheric CO_2 concentration (191.85 ppmv) as recorded in the Taylor dome ice core [*Indermühle et al.*, 2000]. The atmospheric concentrations of CH_4 and N_2O were prescribed to LGM values, according to ice core data [*Brook et al.*, 2000; *Sowers et al.*, 2003]. The LGM boundary forcing adopted here is described in detail by *Timmermann et al.* [2005b] and *Justino et al.* [2005]. After this 2200-yearlong forced simulation the VECODE model was activated and the coupled model ECBilt-CLIO-VECODE-LOCH was forced for an additional 1300 years with glacial greenhouse gas concentrations. The model still used prescribed LGM orbital parameters and glacial topography, as described above. However, albedo and forest fraction were computed directly from VECODE. Thereafter, the atmospheric CO_2 was directly computed from the carbon balance between the atmosphere, the vegetation and the ocean. Another fully coupled 2000-yearlong simulation that was based on the previous forced model run, was conducted using interactive CO_2. As will be documented below this iterative setup generated a quasi steady state LGM simulation with relatively stable CO_2 conditions at 202 ppmv and a weak trend of 4 ppmv per 1000 years. For the short freshwater perturbation experiments analyzed in this study, we anticipate that this weak CO_2 trend will not affect our main conclusions.

3.2. Freshwater Flux Experiments

[12] To study the background state dependence of the biogeochemical response to freshwater perturbations we conducted water hosing experiments under preindustrial (FC) and under LGM conditions (FL). To mimic a typical Heinrich event, anomalous freshwater was injected into the northern North Atlantic (55°W–10°W, 50°N–65°N). The overall duration of the freshwater perturbation was 200 years. The freshwater flux increased linearly during the first 100 years to 2 Sv (1 Sv = 10^6 m^3 s^{-1}), and decreased at a similar rate in the following 100 years to return to unperturbed conditions (Figure 1). The total amount of anomalous freshwater released in these experiments amounts to 6.3 × 10^6 km^3, which is equivalent to a global sea level rise of around 17.5m. Following the freshwater perturbation the simulations FC and FL continued for another 800 years.

4. Results

4.1. Preindustrial and LGM Control Simulations

4.1.1. Climate Mean State

[13] As demonstrated by *Driesschaert* [2005] the preindustrial and the present-day climate states are simulated quite realistically by LOVECLIM, given the reduced

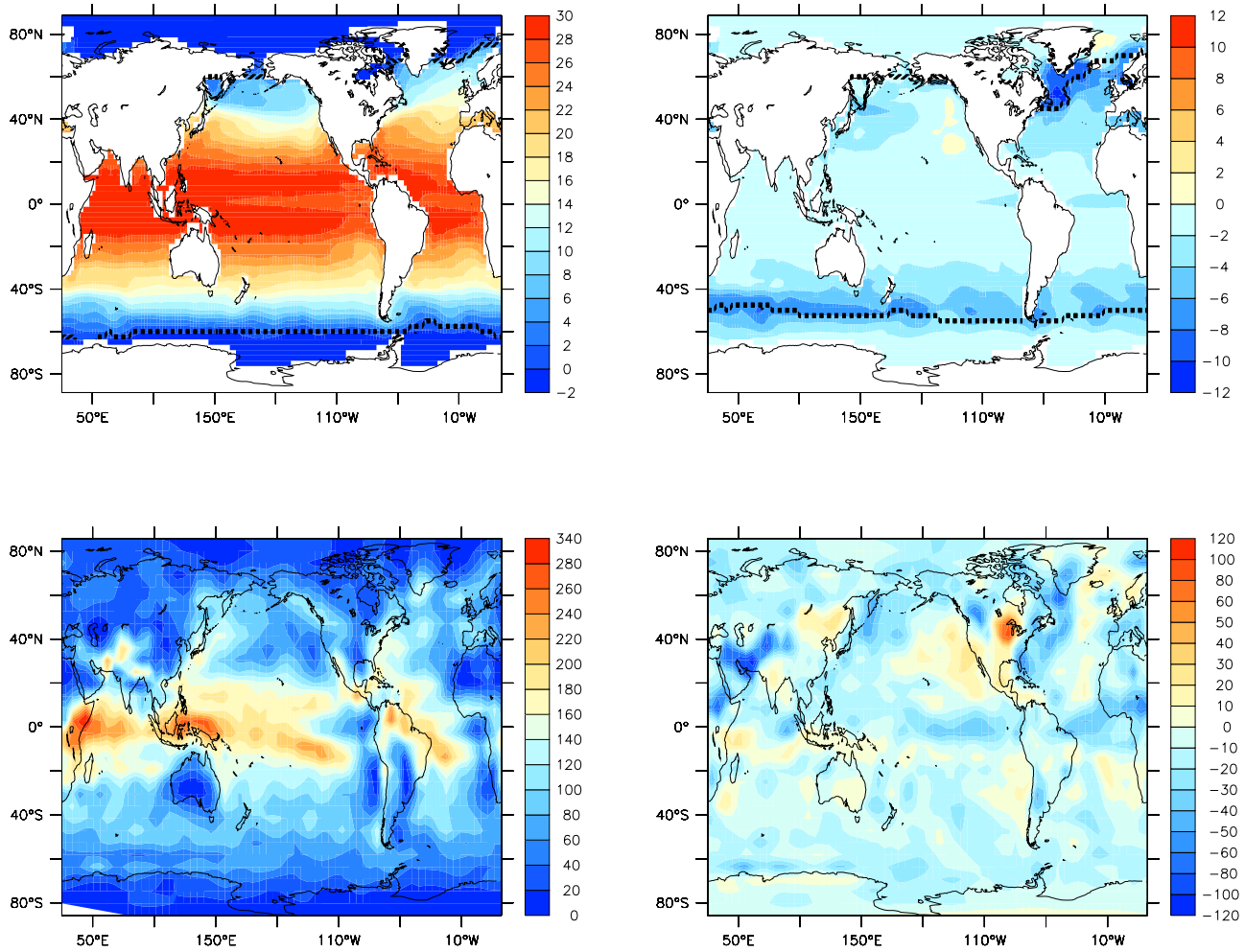

Figure 2. (top) Sea surface temperature (°C) averaged over the last 20 years of the (left) PIN run and (right) difference between the long-term annual mean SST of the LGM experiment and the PIN run (in both simulations SST is averaged over the last 20 years). The dashed line represents the sea ice contour (average of the last 20 years of each run) corresponding to an annual mean height of 0.1 m. (bottom) Same as top plots but for annual mean precipitation (cm a^{-1}).

complexity of the model. Here only the main characteristics of the carbon cycle model and model existing biases of the control climate state will be reviewed. Figure 2 reveals that the simulated zonal mean temperature gradient in the tropical Pacific is not captured realistically, in comparison with the *Reynolds and Smith* [1995] observations (not shown). This can be partly attributed to an underestimation of the tropical air-sea coupling strength, owing mostly to the low atmospheric resolution, and a diffuse thermocline. Furthermore, we see relatively weak temperature fronts near the western boundary currents, another typical feature of coarse-resolution ocean models. While the extratropical westerlies are captured qualitatively well, the simulated tropical trade winds are too zonal. Precipitation is underestimated in the tropical and storm track regions in comparison with the observational records of *Janowiak and Xie* [1999]. Another bias that might affect our modeling results is a positive precipitation bias in tropical eastern Africa, that can be explained in terms of an underestimation of important orographic features in the T21 resolution.

[14] The simulated strength of the preindustrial Atlantic meridional overturning circulation (AMOC) below 500 m amounts to about 27 Sv in the Atlantic (Figure 1), which is somewhat higher than recent observational estimates of 18 ± 5 Sv by *Talley et al.* [2003].

[15] Our simulated LGM climate state is characterized by a global surface air cooling of 4.2°C, with respect to the preindustrial state (Table 1). A more detailed review of the LGM climate state simulated in different versions of ECBilt-Clio and ECBilt-Clio-VECODE is given by *Timmermann et al.* [2004], *Justino et al.* [2005] and *Roche et al.* [2006], respectively. (In comparison to the LGM simulation conducted by *Roche et al.* [2006], we use the ICE4G paleotopography, instead of the ICE5G reconstruction. Furthermore, we employ a higher sensitivity of the

Table 1. Mean Annual Value of Some Climatic and Carbon Cycle Variables Averaged Over the Last 50 Years of the PIN and LGM Runs and Averaged From Years 80 to 100 for FC and FL[a]

	PIN	FC	LGM	FL
AMOC, Sv	26.6	4.0	26.1	3.8
T surface, °C	15.7	14.5	11.5	10.2
SST, °C	18.7	18.25	16.6	16.2
pCO_2a, ppmv	281.8	296.5	201.6	204.3
Δflux $CO_{2\ atm-ocean}$ Gt C a^{-1}	-	0.344	-	0.339
Export production, g C m^{-2} a^{-1}	18.6	16.0	19.6	19.1
PO_4^{3-} (0–120 m), μmol L^{-1}	0.63	0.47	0.76	0.63
DIC (1000–5500 m), μmol L^{-1}	2376	2395	2709	2718

[a]AMOC represents the maximum strength of the overturning circulation in Sv; T surface and SST are the surface air temperature and the sea surface temperature, respectively, in degrees Celsius averaged over the whole globe; pCO_2a is the atmospheric CO_2 content in ppmv; Δflux $CO_{2\ atm-ocean}$ is the anomalous flux of CO_2 from the atmosphere to the ocean in Gt C a^{-1} for FC and FL compared to PIN and LGM, respectively; export production is averaged over all the basins in g C m^{-2} a^{-1}; PO_4^{3-} is the phosphate content averaged over the euphotic zone (0–120 m) in μmol L^{-1}; and dissolved inorganic carbon (DIC) is averaged over the deep ocean in μmol L^{-1}.

longwave radiation to CO_2 changes and neglect sea level changes, changes of the river routing, Antarctic iceberg calving and atmospheric dust loading.)

[16] The largest glacial temperature anomalies are found near the Laurentide and Eurasian ice sheets. Simulated glacial surface air temperatures drop by 15°C to 30°C in the northern extratropics. The equatorward extension of the sea ice in the Southern Hemisphere leads to a decrease of surface temperatures of about 6°C to 15°C. The tropical regions, however, experience only a moderate annual surface cooling of 1°C–3°C, mostly due to the atmospheric CO_2 reduction and due to remote effects from the glacial ice sheets [*Timmermann et al.*, 2004].

[17] SST anomalies in the North Atlantic attain values of up to 8°C (Figure 2) which is in good agreement with latest glacial SST reconstructions [*Weinelt et al.*, 2003; *Pflaumann et al.*, 2003]. SST differences around Antarctica compare well with LGM reconstructions of *Gersonde et al.* [2005]. Tropical SSTs are 1°C to 3°C lower than for the preindustrial state. This also compares favorably with paleoreconstructions of *Kucera et al.* [2005], *Pflaumann et al.* [2003] and *Koutavas et al.* [2002], but is at odds with other tropical SST estimates [*Guilderson et al.*, 2001; *Lea et al.*, 2003; *Nürnberg et al.*, 2000; *Visser et al.*, 2003; *Kienast et al.*, 2001; *Rühlemann et al.*, 1999; *Rosenthal et al.*, 2003].

[18] Both the presence of large orographic barriers and the associated modification of the atmospheric eddy momentum fluxes, as well as the intensified LGM SST gradient lead to an intensification of the trade winds (Figure 3) with implications for the subtropical cell transports and evaporative cooling in the tropical regions. The general cooling of the Earth's atmosphere under glacial conditions leads to a reduced capacity of the atmosphere to hold moisture. This causes a drop of global precipitation by 11 cm a^{-1} during the LGM (Figure 2). In particular dry areas such as the southern border of the Sahara, the Middle East and Far East, the Tibetan plateau as well as central Greenland experience a drop of annual mean precipitation of about 50%. Other areas such as the southern border of the Laurentide ice sheet experience a regional increase in precipitation, which is suggestive of a positive feedback that helps to maintain the glacial ice sheets.

[19] A direct comparison between modeled LGM ocean states and LGM reconstructions [*McManus et al.*, 2004; *Gherardi et al.*, 2005] is not straight forward. This task is rendered difficult by the transient nature of the LGM. As noted by *Timmermann et al.* [2004], LGM simulations are designed as steady state experiments, whereas the observed LGM state occurred about 2000 years after the long-lasting glacial meltwater pulse Heinrich II. It is unclear whether the AMOC was still recovering from this perturbation, or whether it had already reached a new equilibrium state which could be directly compared with steady state paleomodel simulations. Our simulated vigorous glacial Atlantic overturning with an amplitude of about 26 Sv compares well with the simulation of *Roche et al.* [2006] and exhibits

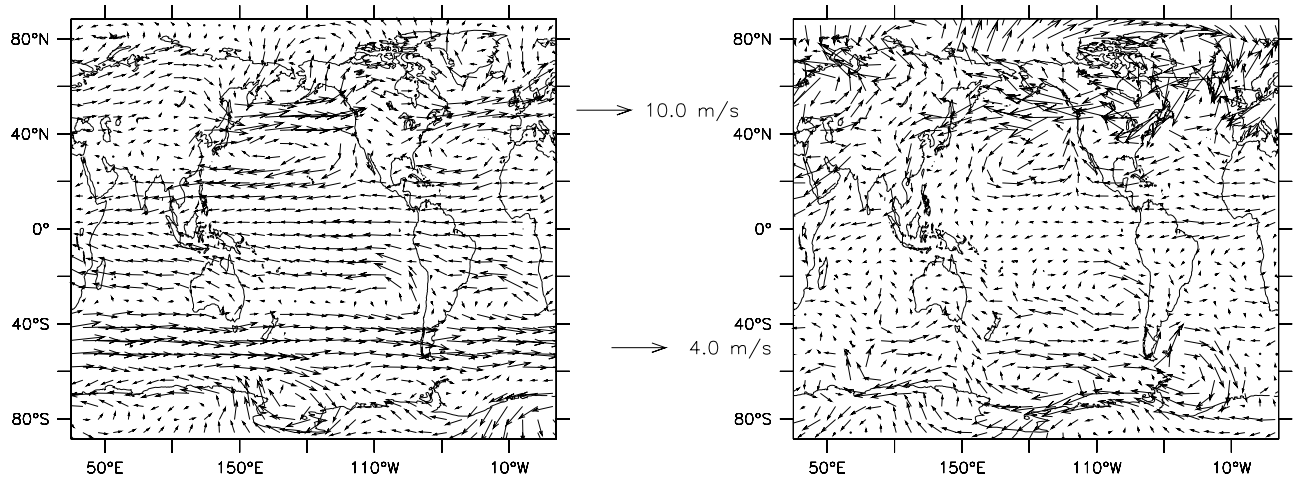

Figure 3. Same as Figure 2 but for annual mean wind velocity (m s^{-1}) at 800 mbar. The reference vector is (left) 10 m s^{-1} for PIN conditions and (right) 4 m s^{-1} for the LGM anomaly.

also a southward displacement of the deepwater formation areas. *Roche et al.* [2006] argue that this finding is not inconsistent with available proxy data, although a meaningful comparison may be hampered by the fact that the observed LGM state was probably not an equilibrium state.

4.1.2. Carbon Cycle

[20] The simulated mean atmospheric CO_2 concentration during the fully coupled PIN amounts to about 282 ppmv. The standard deviation of the CO_2 concentration due to interannual variability attains values of up to 2 ppmv. The partitioning of the preindustrial carbon reservoirs compares well with present-day estimates: While the terrestrial biosphere holds about 2050 Gt C in PIN, about 39,100 Gt C are stored in the ocean. Present-day estimates of these reservoirs are 2000 Gt C and 38,100 Gt C [*Intergovernmental Panel on Climate Change*, 2001], respectively. *Houghton* [1999] suggest that land use changes during the nineteenth and twentieth centuries induced a release of about 120 Gt C from the vegetation. Taking this into account, the preindustrial terrestrial reservoir would account for about 2120 Gt C, which is close to our estimate.

[21] For the LGM steady state experiment (LGM) we simulate a quasi-equilibrium atmospheric CO_2 of 202 ppmv. The mean vegetation and ocean carbon stocks are 1370 Gt C and 40,000 Gt C, respectively. Recent reconstructions of the LGM terrestrial carbon stock were based on $\delta^{13}C$ values of calcite shells of benthic foraminifera [*Duplessy et al.*, 1988; *Curry et al.*, 1988; *Bird et al.*, 1994] as well as on pollen analysis [*Crowley*, 1995; *Adams and Faure*, 1998]. The estimated values for the terrestrial carbon stock range from 1300–1700 Gt C and 600–1300 Gt C, respectively. Our simulated terrestrial carbon reservoir is in the range of these storage estimates and is also in agreement with a vegetation model simulation using the LPJ-DGVM forced with LGM climate conditions [*Joos et al.*, 2004].

[22] The gross biome distribution that we obtain for the PIN and LGM runs (Figure 4) can be directly compared to the reconstructions compiled by *Crowley* [1995] (not shown here). For PIN, the main desert areas are well represented except for Central Asia. Tropical forests dominate the Amazonian basin, the Congo basin as well as Indonesia and Papua New Guinea. However, the dominant biome simulated in southeast Africa is rain forest instead of savanna, and is forest instead of grass in the southwestern part of the United states. During the LGM, the desert fraction increases in north Africa, the Middle East and Central Asia reflecting the drier conditions there, in agreement with paleoreconstructions. On the other hand forest is still the predominant vegetation type in western Europe whereas *Crowley* [1995] suggest that grass covered this area. Most of the main discrepancies between reconstruction and model results can be explained in terms of the mean precipitation biases of our coarse-resolution atmosphere.

[23] In order to show the performances of the marine carbon cycle model (LOCH) under present-day conditions, we compare the difference in partial pressure of CO_2 between the ocean and the atmosphere (ΔpCO_2) as well as the phosphates (PO_4^{3-}) distribution obtained during a present-day run (MOD) with observations. A more thorough comparison of the geochemical tracer distributions is given by L. Menviel et al. (Performances of the marine carbon cycle LOCH under present day conditions, available at http://www.soest.hawaii.edu/oceanography/students/lmenviel/lochperfpdf.pdf, 2007). MOD was obtained by forcing the model with the observed atmospheric CO_2 variations from 1750 to 2000 A.D. [*Keeling et al.*, 1996; *Etheridge et al.*, 1996] starting from the PIN state. Figure 5 displays ΔpCO_2 for the last years of the MOD experiment and the observed data compiled by *Takahashi et al.* [2002]. In both the model and the observations, the Southern ocean, the North Atlantic as well as the North Pacific are a net sink of CO_2 and the equatorial regions, particularly the cold tongue region in the Pacific, are a net source. However, the simulated North Atlantic and North Pacific sinks are a little underestimated. The model also exhibits a source of CO_2 to the atmosphere in the Atlantic and the Indian oceans in the southern boundary regions near the fronts of the southern subtropical gyres at around 40°S. Mismatches between model results and the observations can be largely explain in terms of SST, wind and sea surface salinity (SSS) differences between the fully coupled model solution and the observed climatology. During the LGM (not shown here), the high-latitude CO_2 sinks as well as the low-latitude sources have a greater amplitude than in MOD. Indeed, the colder high latitudes induce an increase in CO_2 solubility, whereas the stronger upwellings at low latitudes enhance the release of CO_2 to the atmosphere.

[24] The PO_4^{3-} distribution averaged over the euphotic zone obtained during MOD (Figure 5) is qualitatively quite similar to the observed one [*Garcia et al.*, 2006]. However, significant quantitative differences can be found in the north Pacific and in the northwestern Indian Ocean, where the simulated PO_4^{3-} is lower by 1 μmol L^{-1} than the observed one. The simulated export production is comparable to the observed one (not shown here), except for the Arabian Sea where it is much lower (Figure 6). The PO_4^{3-} content is higher (by about 0.3 μmol L^{-1}) during the LGM than under preindustrial conditions (PIN) in the southern parts of the Eastern Equatorial Pacific (EEP) and the Eastern Equatorial Atlantic (EEA) (not shown), as can be expected from the intensified trade wind circulation and stronger upwelling. As a result, the marine export production increases by about 15% in the EEP and by about 30% in the EEA (Figure 6). This is consistent with a compilation of export production as recorded in a large number of sediment cores [*Kohfeld et al.*, 2005] which suggests that during the LGM, the export production may have been equal or higher than today outside the non polar areas. Principally because of the sea ice advance, the export production is reduced by 32% in the North Atlantic and 22% in the North Pacific. In the glacial southern Ocean, the PO_4^{3-} content is about 0.4 μmol L^{-1} higher (not shown) because of decreased nutrient utilization. Indeed, the glacial increase in sea ice coverage leads to about 25% decrease in productivity. This result is in agreement with LGM nutrient concentrations in the Antarctic surface ocean as deduced from Cd/Ca ratios in planktonic foraminifera [*Elderfield and Rickaby*, 2000], as well as with the lower primary production estimate made by *Kohfeld et al.* [2005].

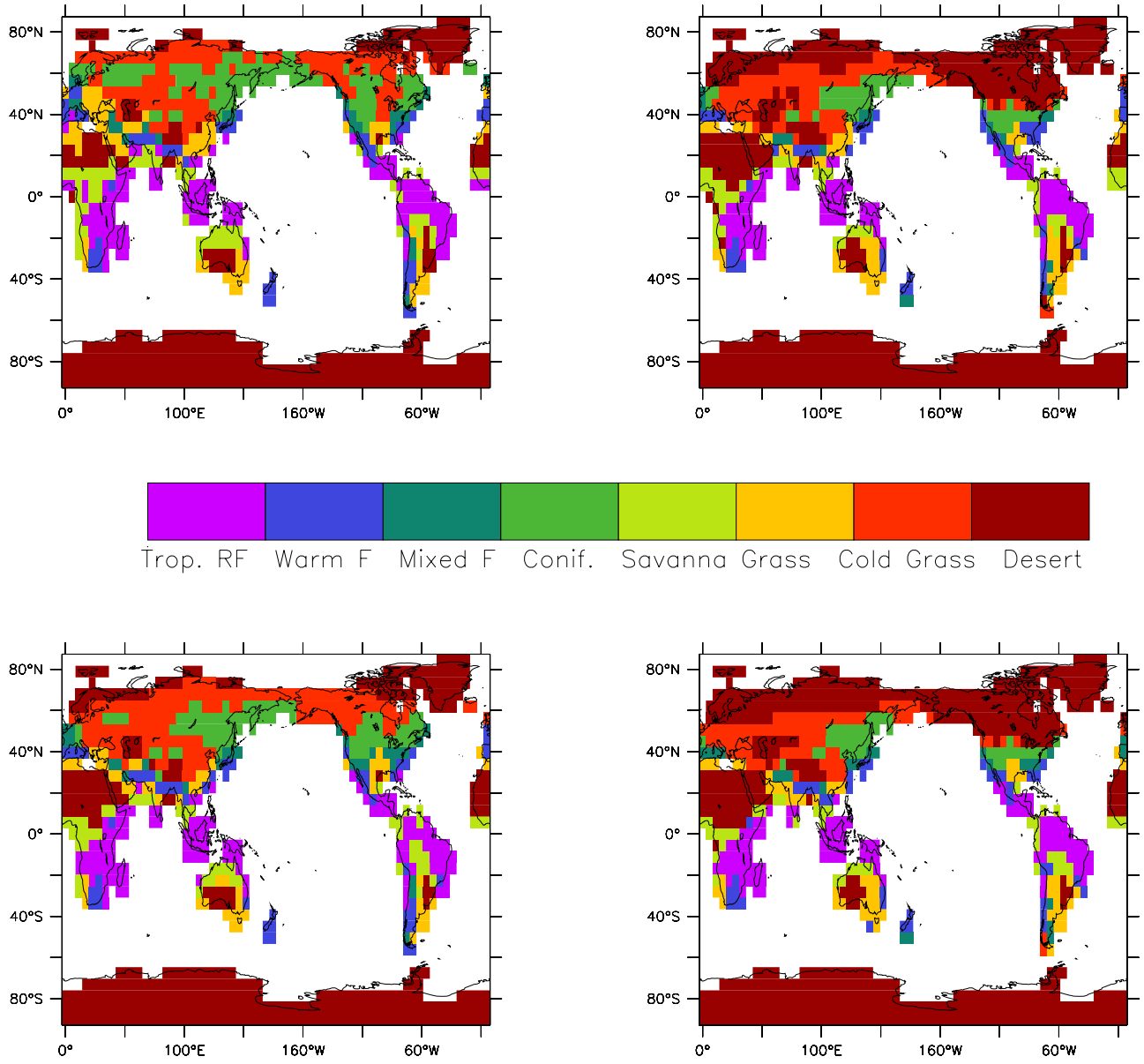

Figure 4. Biome distribution (shown from purple to dark red for tropical rain forest, warm forest, mixed forest, conifers, savanna, grass, cold grass, and desert) for the last 20 years of the (top left) PIN and (top right) LGM runs as well as averaged over the years 180–200 for (bottom left) FC and (bottom right) FL. Only the dominant vegetation biome per grid cell is displayed.

[25] Our LGM model results are qualitatively in good agreement with these paleoreconstructions and with the *Peacock et al.* [2006] synthesis: (1) Simulated LGM PO_4^{3-} values are somewhat larger than for the preindustrial climate, in particular at high latitudes; anomalies at low latitudes if not weakly positive are close to zero. (2) The simulated LGM export production is lower in the polar oceans and of the same order or larger in areas between 50°S and 50°N.

4.2. Freshwater Flux Experiments

4.2.1. Climate Response

[26] In response to the North Atlantic anomalous freshening, the AMOC gradually decreases from a maximum strength of about 26 Sv to a minimum value of around 4 Sv for both the freshwater flux experiment starting from a preindustrial climate state (FC) and the one using LGM boundary conditions (FL) (Figure 1). Whereas the preindustrial AMOC recovers completely after about 600 years, the LGM AMOC recovers already after 400 years. This change in glacial hysteresis behavior has been described in detail by *Krebs and Timmermann* [2007].

[27] Similar to other recent CGCM water hosing experiments [*Stouffer et al.*, 2006; *Timmermann et al.*, 2007], the weakening of the AMOC leads to a substantial cooling in the North Atlantic (Figure 7). While, the North Atlantic cooling is more pronounced in the FC simulation, the Southern Hemispheric warming of up to 2°C is comparable

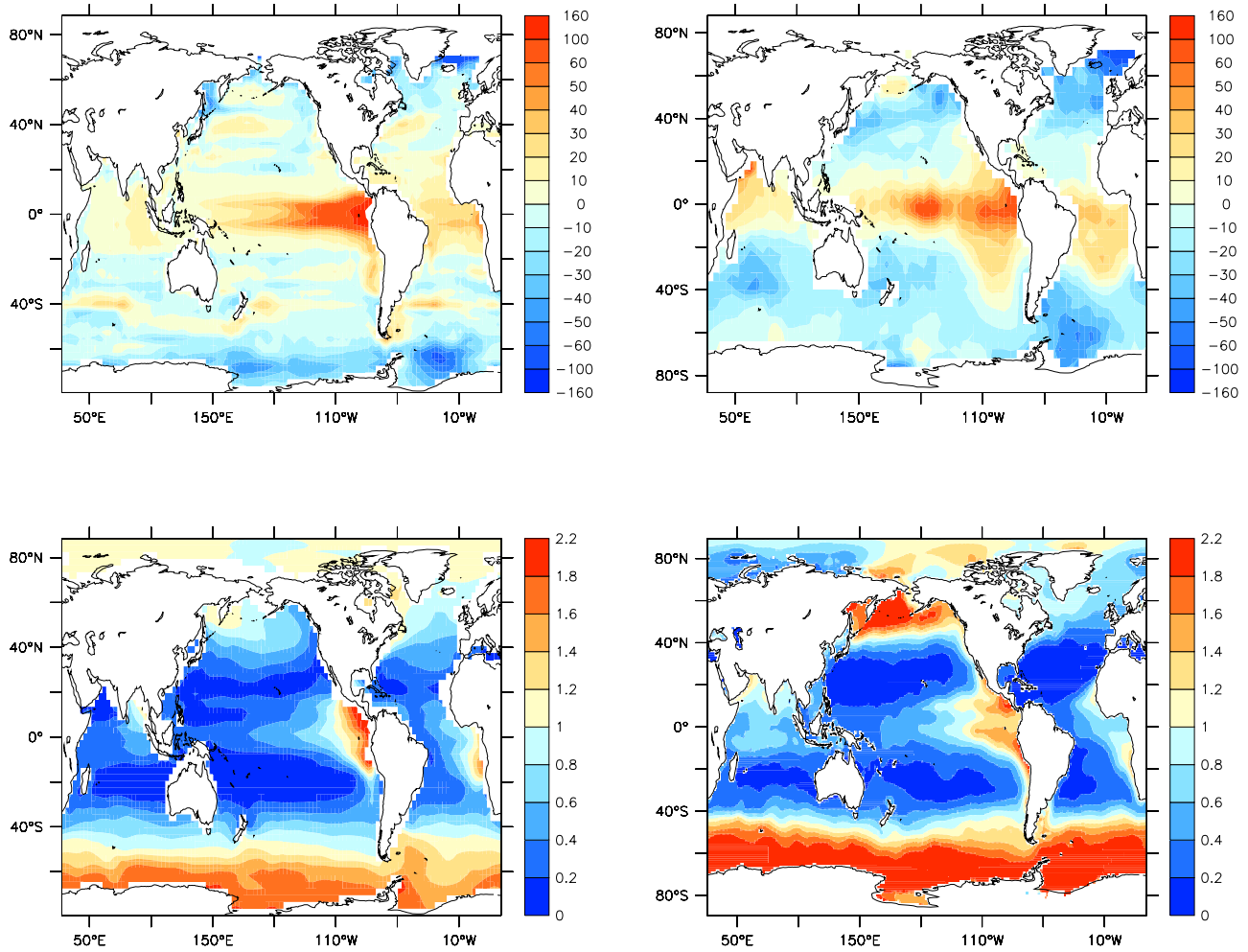

Figure 5. (top) Annual mean air-sea differences in CO_2 partial pressure (μatm) for (left) MOD and (right) the *Takahashi et al.* [2002] reconstructions. (bottom) Simulated long-term annual mean phosphate concentration (μmol L^{-1}) averaged over the euphotic zone (0–120 m) for (left) MOD and (right) the observed annual mean phosphate concentration averaged over the euphotic zone (0–120 m) [from *Garcia et al.*, 2006] is shown.

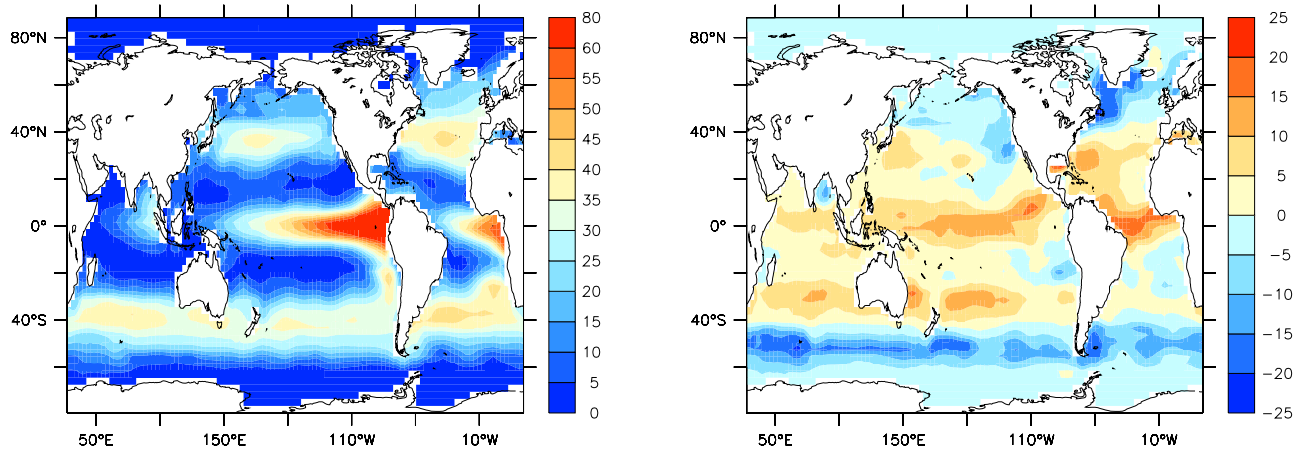

Figure 6. Annual marine export production (g C m^{-2} a^{-1}) averaged over the euphotic zone for (left) the last 20 years of the PIN run and (right) LGM anomalies compared to the last 20 years of the PIN.

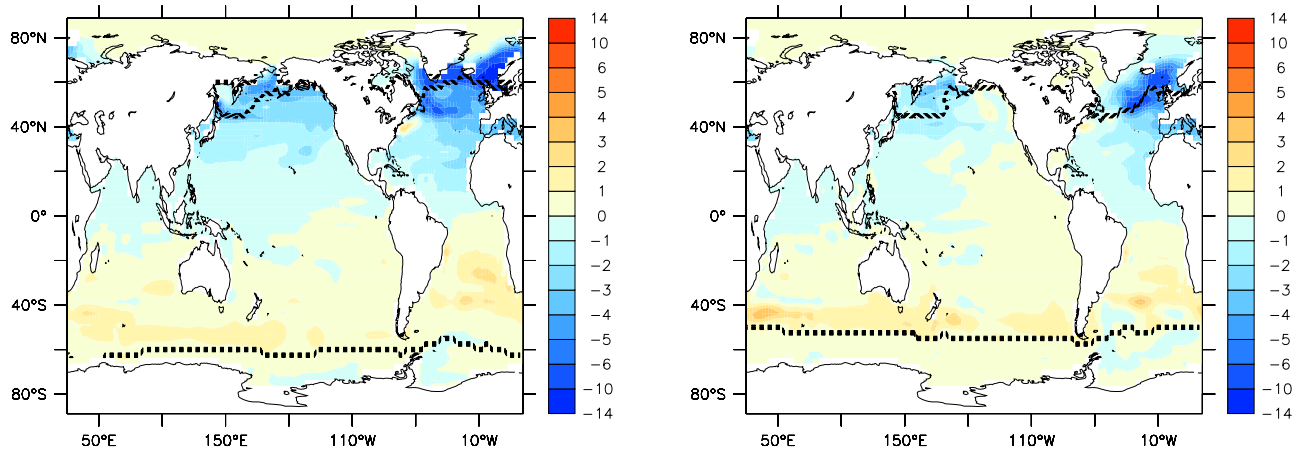

Figure 7. Annual mean sea surface temperatures (SST) anomalies (°C) for (left) FC-PIN and (right) FL-LGM. The SST have been averaged over the years 180–200 for FC and FL and averaged over the last 20 years for PIN and LGM. The dashed line corresponds to the annual mean sea ice height of 0.1 m in FC and FL (averaged over the years 180–200).

in both FC and FL. The Northern Hemispheric sea ice moves equatorward in both FC and FL by about 5°–10°, whereas only small sea ice anomalies are simulated in the Southern Hemisphere. The interhemispheric cooling asymmetry induced by weakening of the AMOC leads to an intensification of the northeasterly trade wind circulation in the Northern Hemisphere (Figure 8) and the establishment of a dipole in the precipitation field. This dipole-like pattern is associated with a southward shift of the Intertropical Convergence Zone (ITCZ) (Figure 9). The physical mechanisms responsible for this ITCZ shift have been described in detail by *Broccoli et al.* [2006], *Timmermann et al.* [2005a], *Zhang and Delworth* [2005] and *Krebs and Timmermann* [2007]. The tropical Atlantic precipitation anomaly is more pronounced in the FC simulation (Figure 9) because the preindustrial atmosphere is warmer and can accumulate more moisture than the glacial atmosphere.

4.2.2. Vegetation Response

[28] During the weakened AMOC state, the drier and colder conditions in the Northern Hemisphere lead to significant changes in the vegetation patterns, and to the dominance of plants that are more adapted to such climatic conditions. In FC, a perennial snow cover leads to a reduction of forest and grass over Scandinavia (Figure 4). Grass is substituted by forest over some parts of northeastern Europe, Siberia and north America and the desert spreads over northern Europe. In the Sahel, desert replaces savanna and in northern South America savanna replaces forest. The most important vegetation and carbon storage changes occur in the tropical latitudinal band 5°S–10°N, both in FC and FL.

[29] Because of increased precipitation in the Southern Hemisphere, more carbon-rich vegetation can be main-

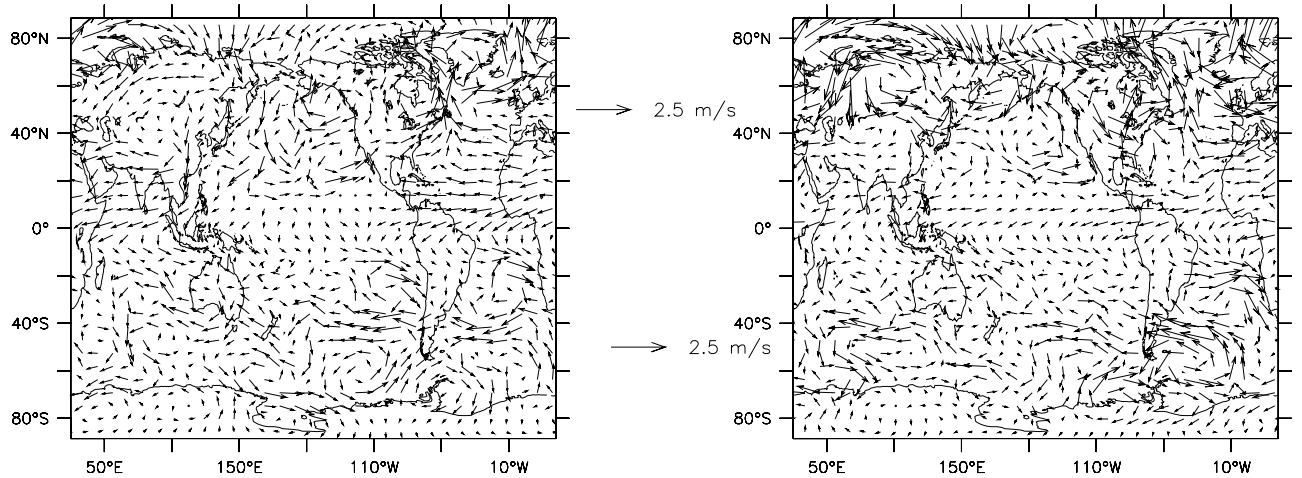

Figure 8. Same as Figure 7 but for annual mean wind velocity anomalies (m s^{-1}) at 800 mbar for (left) FC and (right) FL.

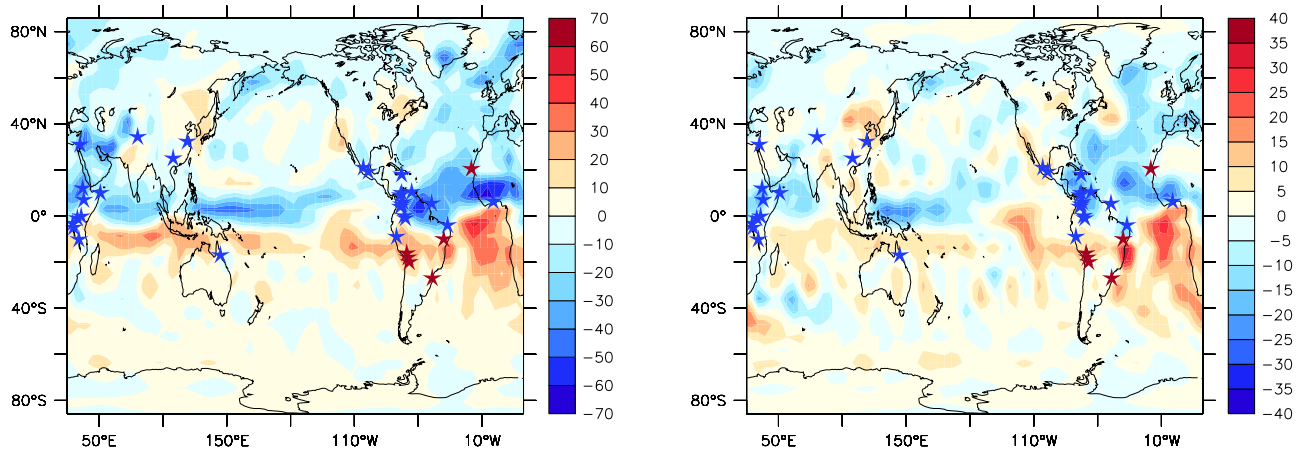

Figure 9. Precipitation anomalies (cm a^{-1}) for (left) FC-PIN and (right) FL-LGM compared to precipitation paleoproxy data (stars). The blue stars indicate a drier climate, and the red stars indicate a wetter climate. See text for references.

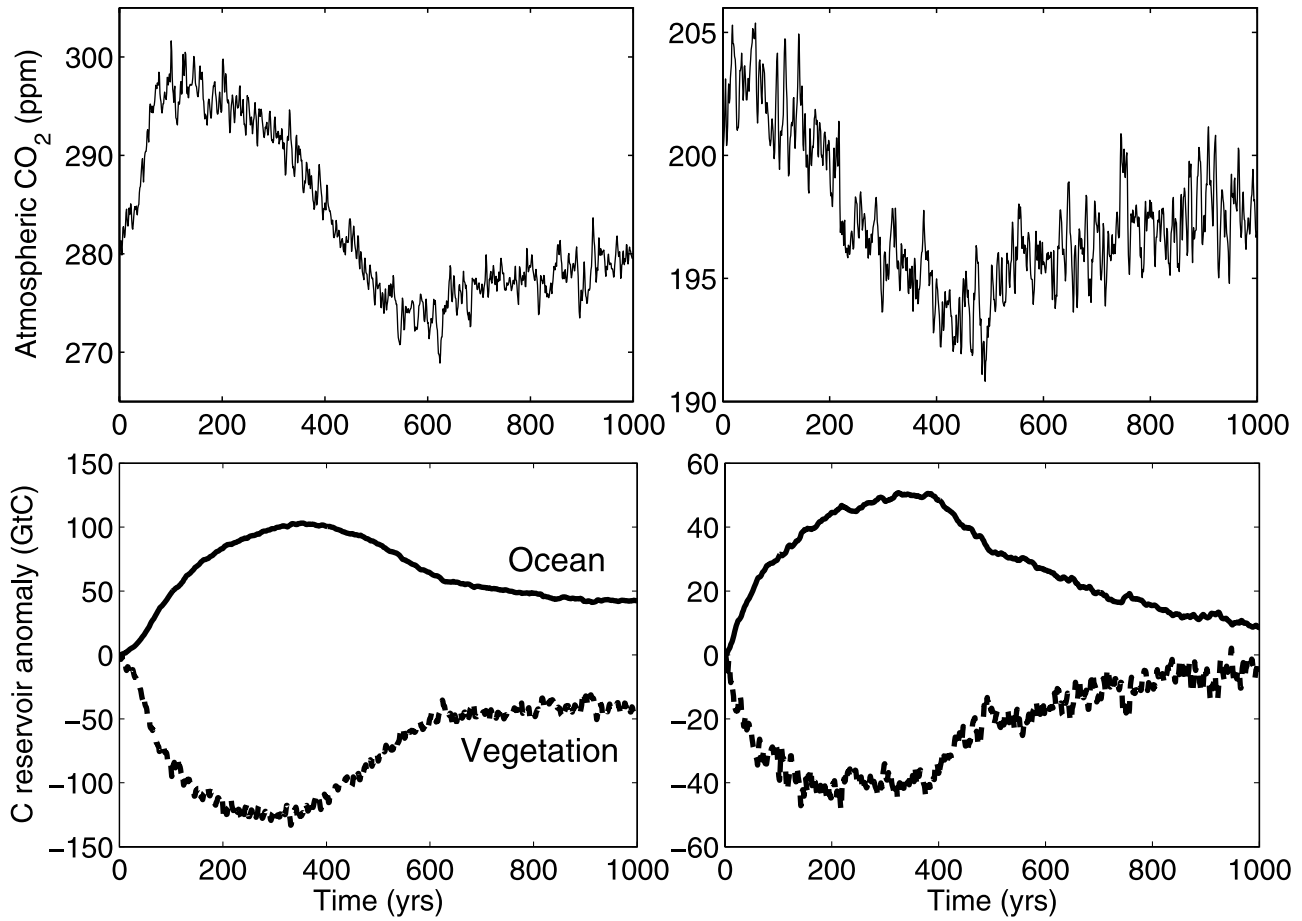

Figure 10. (top) Atmospheric CO_2 content (ppm) for the (left) FC and (right) FL runs. (bottom) Carbon reservoir anomalies (Gt C) for the ocean (solid line) and the vegetation (dashed line) for (left) FC and (right) FL are shown.

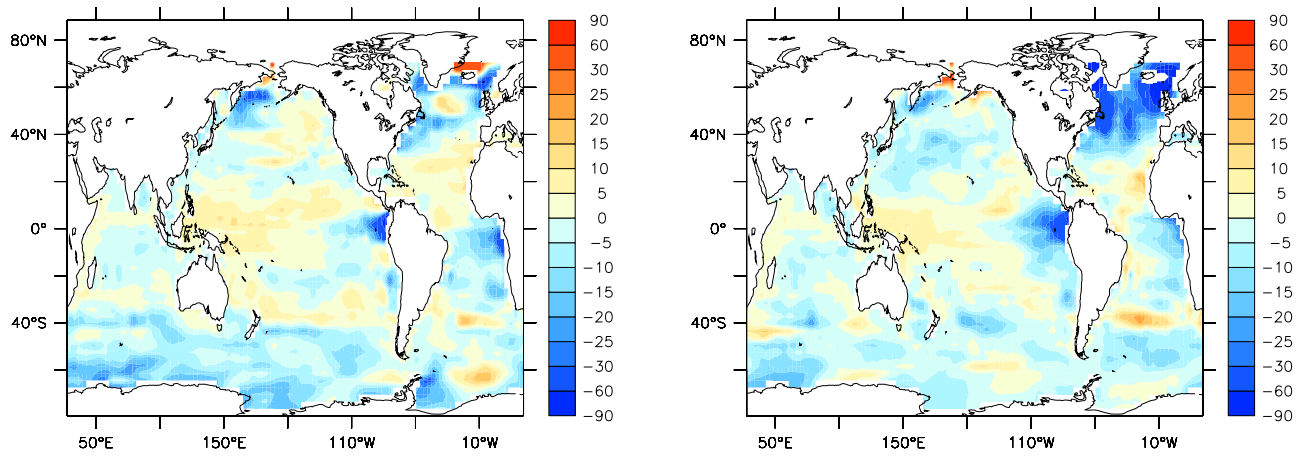

Figure 11. Anomalies of partial pressure of CO_2 differences (μatm) between the ocean and the atmosphere for (left) FC-PIN and (right) FL-LGM averaged over the years 180–200.

tained, leading to an increase of terrestrial carbon stocks in southern Brazil, Paraguay, northern Australia as well as southwest Africa. For the preindustrial experiment FC, the decrease in terrestrial carbon storage in the Northern Hemisphere outweighs the increase in the Southern Hemisphere; the net result being the release of up to 130 Gt C during the first 300 years of the experiment (Figure 10). When the AMOC recovers its initial strength, there is no longer any precipitation anomaly and the vegetation takes up some of the carbon previously released. After the complete recovery of the AMOC in FC, the vegetation carbon stock does not fully recover, leaving a terrestrial deficit of 50 Gt C as compared to the control state.

[30] As documented in Figure 4, similar vegetation changes can be observed in FL. However, because of the cold and dry background climate of the LGM as well as the reduced precipitation anomalies, the amplitude of the vegetation anomalies is smaller in FL than in FC. In FL, the terrestrial carbon reservoir only releases 40 Gt C during the glacial Heinrich event (Figure 10). Furthermore, the original carbon stock in the continental vegetation bounces back within a few centuries to its original value.

4.2.3. Chemical and Biological Response of the Ocean

[31] In the first stages of the AMOC weakening, colder and fresher surface waters in the Northern Hemisphere lead to an enhanced CO_2 solubility in the ocean, which can efficiently buffer the excess CO_2 released by the vegetation. As estimated from the *Takahashi et al.* [1993] relationship, the global temperature decrease leads to a pCO_2 drop of 5 ppmv for FC and 3.4 ppmv for FL. During the first 200 years, the net flux of carbon is from the atmosphere to the ocean (Table 1) both in the FC and FL experiments. As can be seen in Figure 11, the colder climate is associated with an increase in the area of the high-latitude CO_2 sinks. Moreover, weaker upwelling in the EEP and EEA lead to a reduction of the CO_2 release to the atmosphere. The oceanic carbon reservoir increases less in FL than in FC because the smaller terrestrial carbon release leads to a lower atmospheric CO_2 content.

[32] During the AMOC shutdown stages carbon sequestration in the deep ocean is more efficient because of an enhanced oceanic stratification and an overall reduction of tropical upwelling in the main Southern Hemispheric upwelling zones. In experiment FC (model years 80–100), the DIC values below 1000 m are on average 20 μmol L^{-1} higher than in the PIN run (Table 1).

[33] Because of greater stratification in the North Atlantic, the PO_4^{3-} concentration in surface waters is reduced by about 0.5 μmol L^{-1} (0.2 μmol L^{-1} when integrated over the euphotic zone, Figure 12). This leads to 50% decrease in marine export production in that area. In the preindustrial and LGM control simulations, the strongest mean upwellings occur in both the EEP and EEA because of strong Ekman pumping. The associated supply of nutrients into the euphotic zone leads to large marine primary productivity. Because of the AMOC collapse, the circulation, in both the Atlantic and the Pacific, is dominated by the subtropical cells (STC) and the water upwelled in the equatorial regions originates from the subtropics [*Haarsma et al.*, 2008]. As a result of the northern North Atlantic cooling during the weakened AMOC, the trade winds intensify in the northern tropical Atlantic. Because of the sign change of the Coriolis parameter the southern tropical Atlantic experiences a weakening of the trade winds. Consequently, as it was previously described by *Prange and Schulz* [2004] and *Haarsma et al.* [2008], the upwelling strength is increased north of the equator in the EEA, whereas it is decreased south of the equator. In the EEP, the divergent Ekman transport is enhanced in winter but reduced in summer. The global reduction in the amount of water upwelled and the change in source water lead to a reduction of the nutrient content in the upper 1000 m in favor of an accumulation in the deep ocean, especially in the Atlantic. The amount of PO_4^{3-} brought to the upper ocean in the EEP and south of the equator in the EEA is therefore reduced. As can be seen in Figure 12, in those regions the PO_4^{3-} content of the euphotic zone is reduced by about 0.5 μmol L^{-1} compared to PIN. This results in a decrease of the annual mean export production. However, north of the equator in the EEA, the net effect of the stronger upwelling is a slight increase (8%) in export production. Because of the weaker trade winds in the southern tropics, the upwellings are reduced in the

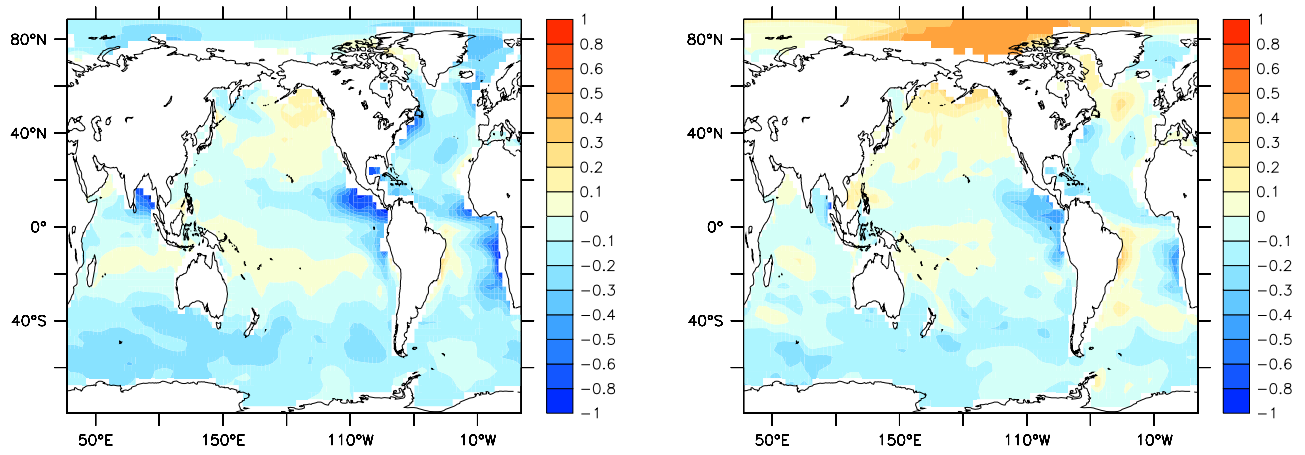

Figure 12. Same as Figure 7 but for annual mean phosphate concentration anomalies (μmol L^{-1}) averaged over the euphotic zone for (left) FC and (right) FL.

southeastern Atlantic and southeastern Pacific. In addition, the Peru (Humboldt) and the Benguela currents are weaker, leading to a reduction in the amount of nutrient rich waters advected from the Southern Ocean to the southeastern Pacific and southeastern Atlantic, respectively. Those regions therefore experience a decrease in export production. While the export production decreases by about 25% in the tropical Pacific because of the weakened AMOC state, the tropical Atlantic export production drops by about 40% (Figure 13). Globally, the export production decreases by about 14% in FC (Figure 13 and Table 1).

[34] Until the beginning of the recovery phase of the AMOC the ocean has taken up about 100 Gt C, part of which is released back to the atmosphere once the effect of the freshwater perturbation ceases. At the end of the simulation FC, the ocean has gained 50 Gt C (Figure 10) because of colder conditions in the Southern Hemisphere. Indeed, at the end of FC, the climate state reaches a slightly different equilibrium than the initial one. The existence of potential multiple equilibria of the carbon climate system deserves a more thorough investigation in a subsequent study.

[35] Under glacial conditions (experiment FL) the overall biogeochemical response to a weakening of the AMOC differs somewhat from that of the preindustrial water hosing experiment FC. The global export production experiences a slight decrease of about 3% (Figure 13 and Table 1). While the response in the tropical oceans is similar to FC, the negative anomalies in the eastern upwelling regions are smaller in FL compared to FC. On the other hand the

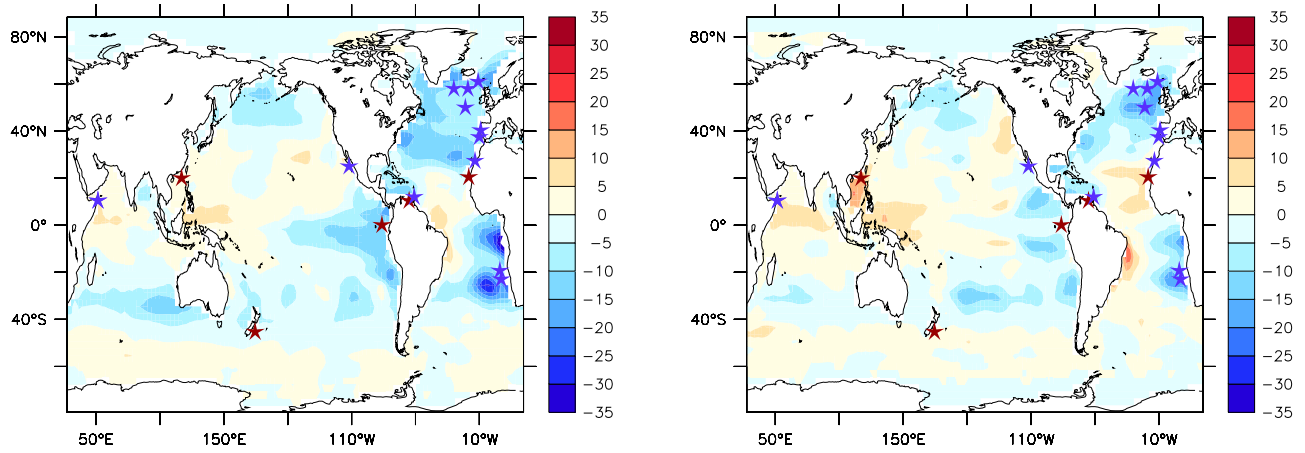

Figure 13. Marine export production anomalies (g C m^{-2} a^{-1}) for (left) FC-PIN and (right) FL-LGM compared to marine primary production paleoproxy data (stars). The blue stars represent lower reconstructed productivity, and the red stars represent larger productivity compared to the reference state during which the anomaly occurs. References from 30°E to 25°E and from north to south are as follows: *Ivanochko et al.* [2005], *Lin et al.* [1999], *Sachs and Anderson* [2005], *Ortiz et al.* [2004], *Kienast et al.* [2006], *Hughen et al.* [1996], *Vink et al.* [2001], *Rasmussen et al.* [2002], *Thomas et al.* [1995], *Pailler and Bard* [2002], *Plewa et al.* [2006], *Haslett and Davies* [2006], and *Little et al.* [1997].

positive productivity anomalies in the western tropical areas are somewhat larger than in FC and in particular off the coast of Brazil and in the south China Sea. This pattern can be explained in terms of stronger equatorial currents that advect nutrients eastward across the Pacific and the Atlantic (Figure 12). The net effect of changes in ocean productivity, solubility and upwelling adds up to a net ocean uptake of 50 Gt C during the weakened AMOC state simulated by FL.

4.2.4. Atmospheric CO_2 Response

[36] Here we decompose the net CO_2 response into vegetation-atmosphere and ocean-atmosphere fluxes. As described above, these individual fluxes are strongly dependent on the climate background conditions. The vegetation response to the AMOC shutdown is quite fast, whereas the ocean biogeochemical conditions adjust on longer timescales to the forcing. This lagged response shapes the time evolution of the atmospheric CO_2 concentration and the carbon stocks, as shown in Figure 10. In FC a shutdown of the AMOC first leads to a fast release of 130 Gt C from the terrestrial reservoir followed by an increase of the ocean reservoir of 100 Gt C with about 30 years lag. When the AMOC starts to recover, the terrestrial carbon storage increases again and therefore leads to an atmospheric CO_2 draw down. For FC, the peak to peak increase in atmospheric CO_2 amounts to about 15 to 20 ppmv (Figure 10). After about 600 years, the atmospheric CO_2 content attains preindustrial values (280 ppmv). The radiative effect of the CO_2 increase further amplifies the development of the bipolar seesaw, as already suggested by *Rohling et al.* [2004]. Indeed, the additional terrestrial CO_2 release warms the southern polar regions by up to 2°–4°C, thereby providing an important element for the bipolar seesaw response.

[37] In the glacial water hosing simulation FL, the vegetation only releases around 40 Gt C and the ocean reservoir increases by 50 Gt C (Figure 10). The ocean lags the vegetation changes by only a few years, which leads to a few ppmv (2–3 ppmv) increase in atmospheric CO_2, after which the oceanic sink of CO_2 becomes dominant. Overall, the AMOC shutdown under glacial conditions leads to a peak to peak decrease of atmospheric CO_2 of about 10 ppmv.

[38] Our analysis clearly shows that a rather delicate balance exists between the response of the marine and terrestrial carbon cycle. This also suggests that mean state model biases might generate substantial errors in the CO_2 response to a shutdown of the AMOC. Assessing these errors can be done by a careful qualitative comparison between paleoproxy data and model simulations as well as by comparing our results with those obtained from model simulations which include e.g., a more sophisticated vegetation component [*Scholze et al.*, 2003b; *Köhler et al.*, 2005].

5. Discussion and Comparison With Paleoclimate Records

5.1. Climate

[39] A careful validation of our earth system model of intermediate complexity under preindustrial and LGM conditions has revealed that despite the simplicity of the atmospheric and the vegetation component, many features of the climate and biogeochemical state are simulated qualitatively well and in agreement with present-day observations and paleoproxy reconstructions. This includes the LGM climate background state [*Justino*, 2004; *Justino et al.*, 2005; *Roche et al.*, 2006, and references therein], the terrestrial carbon reservoir [*Adams and Faure*, 1998] as well as the biome partitioning under LGM conditions [*Crowley*, 1995].

[40] The freshening of the North Atlantic leads to a temporary shutdown of the AMOC and a substantial reduction of the meridional heat transport in the North Atlantic of about 0.8 PW at 30°N and an increase of the poleward heat transport in the Southern Hemisphere of about 0.5 PW. While the recovery takes about 500 years under preindustrial conditions, it is somewhat faster during glacial conditions (~300 years). The reduction of ocean heat transport in the North Atlantic leads to a substantial cooling of the northern North Atlantic, an equatorward extension of the perennial sea ice cover and an intensification of the northeasterly trade winds. Furthermore, as a result of stronger poleward heat transport in the Southern Hemisphere, the Southern Ocean warms significantly. A reduction of the southeasterly trade winds amplifies this warming because of the wind-evaporation-SST feedback [*Krebs and Timmermann*, 2007]. A substantial weakening of the meridional overturning circulation as simulated in a series of coupled GCMs lead to a global SST reduction of 0.2°C to 1.2°C [*Timmermann et al.*, 2007]. We simulate a global SST decrease of about 0.4°C, which is in agreement with the other GCMs.

[41] The meridional reorganization of the trade wind circulation and the tropical SST gradients lead to a southward shift of the ITCZ. Both in FC and FL the northern tropical band gets drier and the southern tropical band experiences much wetter conditions during the collapsed AMOC state. The simulated precipitation anomaly pattern is qualitatively in good agreement with paleoclimate reconstructions, as illustrated in Figure 9. Lake level studies [*Flores-Diaz*, 1986; *Gasse et al.*, 1990; *Street-Perrot and Perrot*, 1990; *Hodell et al.*, 1991; *Gasse and Van Campo*, 1994; *Bonnefille et al.*, 1995; *VanDerHammen and Hooghiemstra*, 1995; *Johnson et al.*, 2002; *Stager et al.*, 2002; *Adegbie et al.*, 2003; *Scholz et al.*, 2003; *Turney et al.*, 2004; *Lamb et al.*, 2007], geochemical precipitation proxies from marine sediment cores [*Arz et al.*, 1998; *Maslin and Burns*, 2000; *Haug et al.*, 2001; *Ivanochko et al.*, 2005; *Haslett and Davies*, 2006], speleothems [*Wang et al.*, 2001; *Bar-Matthews et al.*, 2003; *Dykoski et al.*, 2005; *Wang et al.*, 2006], as well as tropical ice cores [*Thompson et al.*, 1995] support the notion that the Northern Hemisphere was drier during Heinrich events and/or the YD. Our simulated precipitation increase in South America is also in agreement with recent paleoclimatic records [*Thompson et al.*, 1998; *Baker et al.*, 2001a, 2001b; *Wang et al.*, 2004; *Cruz et al.*, 2005]. The southward shift of the main precipitation bands during weakened AMOC states appears to be a robust feature, both in climate model experiments as well as in paleoreconstructions.

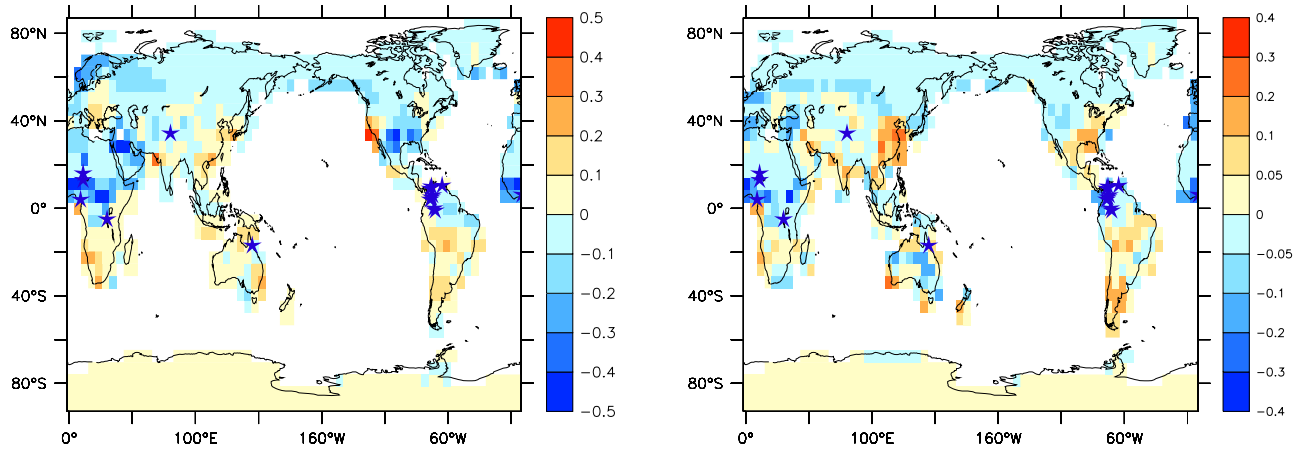

Figure 14. Vegetation primary production anomalies (kg C m^{-2} a^{-1}) for (left) FC-PIN and (right) FL-LGM compared to vegetation paleoproxy data (stars). The stars represent a reconstructed vegetation type that is adapted to a drier climate. See text for references.

5.2. Vegetation Response

[42] The southward shift of the ITCZ induces large-scale vegetation changes in the tropics. In response to an AMOC weakening we simulated changes from savanna to desert in northern Africa as well as a reduction of the forest area in northwestern tropical Africa and the northeastern part of South America. The amplitude of these vegetation anomalies depends strongly on the climate-vegetation background state. Under glacial conditions, vegetation adapted to a drier and colder climate already prevail. The simulated changes of terrestrial carbon stock are therefore smaller under glacial than under preindustrial conditions. For FC, the terrestrial carbon reservoir releases 130 Gt C to the atmosphere, whereas only 45 Gt C are released in FL. Simulated vegetation changes in FC and FL are in qualitative agreement with some pollen studies from equatorial Africa and northern South America that suggest a change toward drier climate vegetation during the YD period [*Gasse and Van Campo*, 1994; *VanDerHammen and Hooghiemstra*, 1995; *Maley and Brenac*, 1998; *Hughen et al.*, 2004] (Figure 14). Indeed, as suggested by *Myneni et al.* [1995], a precipitation reduction in a certain environment leads to a decrease in vegetation primary productivity. The wetter conditions in the Southern Hemisphere do not lead to large changes in the terrestrial carbon storage, except for southwestern Africa and western South America.

[43] These results are in qualitative agreement with the ones obtained by *Köhler et al.* [2005] as well as *Scholze et al.* [2003b] using a more complex vegetation model. Indeed, the main features of the LPJ-DGVM response to a shutdown of the AMOC are a reduction in tree cover north of 55°N, a slight increase in carbon storage due to a southward shift of the tree line around 40°N, a replacement of tropical trees by grass due to drier conditions in the latitudinal band 5°S–15°N and a slight increase in carbon storage between 10°S and 20°S due to greater precipitation. However, for the preindustrial climate, we obtain a terrestrial carbon release of 130 Gt C which is much larger than the 40 Gt C obtained by *Köhler et al.* [2005] but lower than the 180 Gt C simulated by *Scholze et al.* [2003b]. *Köhler et al.* [2005] explained their discrepancy with *Scholze et al.* [2003b] results by differences in the initial climate state. In our simulation the vegetation cover–albedo feedbacks are included, which could be the reason of the larger terrestrial carbon released obtained compared to the *Köhler et al.* [2005] study. The different time evolution of terrestrial carbon stock simulated by *Köhler et al.* [2005] could be partly explained by the difference in the freshwater flux forcing applied. The sensitivity of the terrestrial carbon release to the initial climate state is consistent with the studies of *Köhler et al.* [2005] as well as *Scholze et al.* [2003a] where less carbon is released when starting from a cold climate state because of the dominance of vegetation adapted to drier conditions. However, those results cannot be directly compared to ours as they assumed the same climate anomaly for a freshwater flux experiment starting from a preindustrial climate state as the one starting from a cold climate state. We have demonstrated earlier in this paper that the climate anomalies have qualitatively the same pattern but not the same amplitude, which further amplifies the differences between FC and FL.

[44] The vegetation response is primarily driven by the changes in precipitation and temperature. The agreement between the climate response to a shutdown of the AMOC obtained by different modeling studies [*Broccoli et al.*, 2006; *Krebs and Timmermann*, 2007; *Timmermann et al.*, 2005a; *Zhang and Delworth*, 2005; *Knutti et al.*, 2004] and paleoclimate as well as paleovegetation records suggests that the overall vegetation response pattern is robust.

5.3. Response of the Marine Carbon Cycle

[45] In FC, the strong release of carbon from the terrestrial reservoir induces an increase in atmospheric CO_2, which leads to a higher difference between the atmospheric partial pressure of CO_2 and the one in equilibrium with the surface ocean. The ocean therefore acts as a sink of CO_2. This effect is further amplified by reduced surface water temperature and salinity and hence greater CO_2 solubility. The increase of the oceanic carbon inventory by about 100 Gt C is

however not sufficient to balance the terrestrial release. In FL, the ocean carbon reservoir gains up to 50 Gt C because of increased solubility (Figure 10). This result is contrary to the *Marchal et al.* [1999] study where the CO_2 solubility was reduced because of greater sea surface temperature and salinity. This difference could be due to the fact that *Marchal et al.* [1999] do not use a three-dimensional dynamical atmosphere and only a two-dimensional ocean model.

[46] Figure 13 shows the export production anomalies for FC and FL as well as a compilation of reconstructed changes in primary production for the YD and/or Heinrich events as recorded in marine sediment cores. Export production decreases in the North Atlantic in several sediment cores [*Thomas et al.*, 1995; *deMenocal et al.*, 2000; *Pailler and Bard*, 2002; *Rasmussen et al.*, 2002], consistent with our modeling results for FC and FL as well as with the results of *Schmittner* [2005]. In our model simulations the lower productivity can be explained in terms of a reduced supply of nutrients to the upper ocean due to increased stratification. The increased productivity due to stronger upwelling off the coast of northern Africa in the Atlantic, in particular in FL is in agreement with *Haslett and Davies* [2006] paleorecord. Our modeling results further suggest that one of the areas which exhibits very large changes both of temperature and productivity is the eastern south Atlantic near the coast of Namibia. A drastic drop in export production due to a reduction in the advection of nutrient rich waters has also been obtained by *Schmittner* [2005]. This result is also in agreement with the paleoreconstruction of *Little et al.* [1997]. However, other high-resolution marine productivity records from this area are needed to consolidate the results.

[47] Striking discrepancies between the model experiments and the reconstructions occur in the EEP [*Kienast et al.*, 2006] and the Arabian Sea [*Ivanochko et al.*, 2005]. However, we can only compare our results with single paleorecords from those sites. Other paleoproductivity records would be needed to validate or falsify our results with confidence. In agreement with our study, *Schmittner* [2005] simulate a reduction in the nutrient content of the upper Pacific ocean, and therefore a lower primary productivity in the EEP. However, as the wind-driven changes in upwelling are not taken into account by *Schmittner* [2005], the global effect of wind stress and nutrient source variations cannot be inferred with certainty.

[48] Our model does not include iron atmospheric transport, but the climate anomalies obtained over the North Pacific and Patagonia (the main dust source of the Southern Ocean) does not support any significant change in dust transport. Moreover, an increase in marine primary productivity due to iron fertilization does not necessarily lead to a significant increase in export production [*de Baar et al.*, 2005]. We therefore think that the lack of iron limitation in our model should not significantly impact our results.

5.4. Atmospheric CO_2 Response

[49] Atmospheric CO_2 changes in response to a shutdown of the AMOC are the result of two large opposing carbon fluxes from the vegetation to the atmosphere and from the atmosphere to the ocean. The simulations have shown that the delicate balance between those fluxes can result in quite different atmospheric CO_2 responses. Any qualitative comparison with paleoproxies is, at this stage, associated with large uncertainties.

[50] Variations in atmospheric CO_2 associated with the YD can be reconstructed from ice core records. The analysis of *Monnin et al.* [2001] suggests that the atmospheric CO_2 concentration increased by more than 20 ppmv during the YD. The immediate effect of Heinrich event I (H1) on atmospheric CO_2 is more difficult to assess. As H1 coincides with the onset of the deglaciation [*Marshall and Koutnik*, 2006], which was characterized by large orbital forcing anomalies in the Northern and Southern hemispheres, our idealized experiments FC and FL can not be directly compared with the atmospheric CO_2 record for that time period. Attributing the observed changes of atmospheric CO_2 during 19–14 ka to variations of the AMOC, orographic ice sheet forcing or orbital forcing is difficult and beyond the scope of this paper.

[51] During MIS3 CO_2 varied between 185 and 220 ppmv on a number of different timescales. There is some evidence [*Stauffer et al.*, 1998] that these variations correlated with Heinrich events, although both the exact timing of the Heinrich events as well as of the CO_2 variations is quite uncertain. Furthermore, it has to be noted that early glacial meltwater pulses (Heinrich 6 through C25) [*Chapman and Shackleton*, 1999] occurred on a precessional timescale of 19–23 ka. Orbital forcing might have affected the CO_2 history and may have triggered meltwater pulses independently from each other, resulting in a possible correlation between the CO_2 and meltwater forcing, but no direct causality.

[52] However, the range of the simulated atmospheric CO_2 response (−10 to +20 ppmv) obtained in response of a collapse of the AMOC is reasonable compared to the atmospheric CO_2 variations as recorded in ice cores.

6. Summary

[53] We conducted a series of climate model simulations with an earth system model of intermediate complexity to understand the CO_2 response to a shutdown of the AMOC under preindustrial and glacial background conditions. The AMOC shutdown was induced by a 200-yearlong injection of freshwater into the northern North Atlantic, corresponding to a global sea level rise of roughly 20 m. Strong cooling in the North Atlantic spreads via changes of the atmospheric circulation [*Krebs and Timmermann*, 2007] and leads to an intensification of the northeasterly trade winds. These atmospheric circulation changes are accompanied by a southward shift of the ITCZ, generating drier conditions in the north (5°S–15°N) and wetter conditions in the south (8°S–20°S). Following the reduction of Northern Hemispheric precipitation, the vegetation releases carbon to the atmosphere, a part of which is taken up by the ocean, mainly because of an increased solubility. The atmospheric CO_2 therefore increases by about 15 ppmv when starting from a preindustrial state whereas it decreases by about 10 ppmv when the initial climate state is a glacial one. The

atmospheric CO_2 response is a delicately balanced sum of the terrestrial and marine inventory changes. This emphasizes the importance of the initial climate state on the CO_2 response to large-scale ocean circulation changes. In order to test the robustness of our results, similar simulations should be performed with other earth system models that include both the marine and terrestrial carbon cycle as well as a more comprehensive atmospheric component.

[54] **Acknowledgments.** L. Menviel is supported by the NSF under grant number ATM06-28393, and A. Timmermann and O. Timm are supported by the Japan Agency for Marine-Earth Science and Technology (JAMSTEC) through its sponsorship of the International Pacific Research Center. A. Mouchet acknowledges support from the Belgian Science Policy (BELSPO contract SD/CS/01A). We gratefully acknowledge stimulating discussions with Thomas Stocker (Physics Institute, University of Bern), Kelvin Richards (IPRC), and Richard Zeebe (Department of Oceanography, University of Hawai'i). We thank K. Rodgers, L. Skinner, and an anonymous reviewer for their helpful reviews.

References

Adams, J. M., and H. Faure (1998), A new estimate of changing carbon storage on land since the Last Glacial Maximum, based on global land ecosystem reconstruction, *Global Planet. Change*, *16–17*, 3–24.

Adegbie, A. T., R. R. Schneider, U. Röhl, and G. Wefer (2003), Glacial millennial-scale fluctuations in central African precipitation recorded in terrigenous sediment supply and freshwater signals offshore Cameroon, *Palaeogeogr. Palaeoclim. Palaeoecol.*, *197*, 323–333.

Arz, H. W., J. Pätzold, and G. Wefer (1998), Correlated millennial-scale changes in surface hydrography and terrigenous sediment yield inferred from last-glacial marine deposits off northeastern Brazil, *Quat. Res.*, *50*, 157–166.

Baker, P. A., C. A. Rigsby, G. O. Seltzer, S. C. Frisk, T. K. Lowenstein, N. P. Bacher, and C. Veliz (2001a), Tropical climate changes at millennial and orbital timescales on the Bolivian Altiplano, *Nature*, *409*, 698–701.

Baker, P. A., G. O. Seltzer, S. C. Frisk, R. B. Dunbar, M. J. Grove, P. M. Tapia, S. L. Cross, H. D. Rowe, and J. P. Broda (2001b), The history of South American tropical precipitation for the past 25,000 years, *Science*, *291*, 640–643.

Bar-Matthews, M., A. Ayalon, M. Gilmour, A. Matthews, and C. J. Hawkesworth (2003), Sea-land oxygen isotopic relationships from planktonic foraminifera and speleothems in the eastern Mediterranean region and their implication for paleorainfall during interglacial intervals, *Geochim. Cosmochim. Acta*, *67*, 3181–3199.

Berger, A. (1978), Long term variations of daily insolation and Quaternary climate change, *J. Atmos. Sci.*, *35*, 2362–2367.

Bird, M. I., J. Lloyd, and G. D. Farquhar (1994), Terrestrial carbon storage at the LGM, *Nature*, *371*, 566.

Blunier, T., and E. J. Brook (2001), Timing of millennial-scale climate change in Antarctica and Greenland during the last glacial period, *Science*, *291*, 109–112.

Bond, G. (1993), Correlations between climate records from North Atlantic sediments and Greenland ice, *Nature*, *365*, 143–147.

Bond, G., H. Heinrich, W. Broecker, and L. Labeyrie (1992), Evidence of massive discharges of icebergs into the North Atlantic during the last glacial period, *Nature*, *360*, 245–249.

Bonnefille, R., G. Riollet, G. Buchet, M. Icole, R. Lafont, M. Arnold, and D. Jolly (1995), Glacial/interglacial record from intertropical Africa, high resolution pollen and carbon data at Rusaka Burundi, *Quat. Sci. Rev.*, *14*, 917–936.

Broccoli, A. J., K. A. Dahl, and R. J. Stouffer (2006), Response of the ITCZ to Northern Hemisphere cooling, *Geophys. Res. Lett.*, *33*, L01702, doi:10.1029/2005GL024546.

Broecker, W. S. (1998), Paleocean circulation during the last deglaciation: A bipolar seesaw?, *Paleoceanography*, *13*, 119–121.

Brook, E. J., S. Harder, J. Severinghaus, E. J. Steig, and C. M. Sucher (2000), On the origin and timing of rapid changes in atmospheric methane during the last glacial period, *Global Biogeochem. Cycles*, *14*, 559–572.

Brovkin, V., A. Ganapolski, and Y. Svirezhev (1997), A continuous climate-vegetation classification for use in climate-biosphere studies, *Ecol. Modell.*, *101*, 251–261.

Cacho, I., J. O. Grimalt, C. Pelejero, M. Canals, F. J. Sierro, J. A. Flores, and N. Shackleton (1999), Dansgaard-Oeschger and Heinrich event imprints in Alboran Sea paleotemperatures, *Paleoceanography*, *14*, 698–705.

Campin, J. M., and H. Goosse (1999), A parameterization of dense overflow in large-scale ocean models in z coordinate, *Tellus, Ser. A*, *51*, 412–430.

Carlson, A. E., P. U. Clark, B. A. Haley, G. P. Klinkhammer, K. Simmons, E. J. Brook, and K. J. Meissner (2007), Geochemical proxies of North American freshwater routing during the Younger Dryas cold event, *Proc. Natl. Acad. Sci. U. S. A.*, *104*, 6556–6561.

Chapman, M. R., and N. J. Shackleton (1999), Global ice-volume fluctuations, North Atlantic ice-rafting events, and deep-ocean circulation changes between 130 and 70 ka, *Geology*, *27*, 795–798.

Crowley, T. J. (1995), Ice-age terrestrial carbon changes revisited, *Global Biogeochem. Cycles*, *9*, 377–389.

Crowley, T. J., and S. K. Baum (1997), Effect of vegetation on an ice-age climate model simulation, *J. Geophys. Res.*, *102*, 16,463–16,480.

Cruz, F. W., Jr., S. J. Burns, I. Karmann, W. D. Sharp, M. Vuille, A. O. Cardoso, J. A. Ferrari, P. L. Silva Dias, and O. Viana Jr. (2005), Insolation-driven changes in atmospheric circulation over the past 116,000 years in subtropical Brazil, *Nature*, *434*, 63–66.

Curry, W. B., J. C. Duplessy, L. Labeyrie, and N. J. Shackleton (1988), Changes in the distribution of $\delta^{13}C$ of deep water ΣCO_2 between the last glaciation and the Holocene, *Paleoceanography*, *3*, 317–341.

Dansgaard, W., S. J. Johnsen, and H. B. Clausen (1993), Evidence for general instability of past climate from a 250-kyr ice-core record, *Nature*, *364*, 218–220.

de Baar, H. J. W., et al. (2005), Synthesis of iron fertilization experiments: From the Iron Age in the Age of Enlightenment, *J. Geophys. Res.*, *110*, C09S16, doi:10.1029/2004JC002601.

deMenocal, P. B., J. Ortiz, T. Guilderson, and M. Sarnthein (2000), Coherent high- and low-latitude climate variability during the Holocene warm period, *Science*, *288*, 2198–2202.

Driesschaert, E. (2005), Climate change over the next millennia using LOVECLIM, a new Earth system model including the polar ice sheets, Ph.D. thesis, Univ. cath. de Louvain, Louvain-la-Neuve, Belgium. (Available at http://edoc.bib.ucl.ac.be:81/ETD-db/collection/available/BelnUcetd-10172005-185914/)

Duplessy, J. C., N. J. Shackleton, R. G. Fairbanks, L. Labeyrie, D. Oppo, and N. Kallel (1988), Deepwater source variations during the last climate cycle and their impact on the global deepwater circulation, *Paleoceanography*, *3*, 343–360.

Dykoski, C. A., R. L. Edwards, H. Cheng, D. Yuan, Y. Cai, M. Zhang, Y. Lin, and J. Qing (2005), A high-resolution, absolute-dated Holocene and deglacial Asian monsoon record from Dongge Cave, China, *Earth Planet. Sci. Lett.*, *233*, 71–86.

Elderfield, H., and R. E. M. Rickaby (2000), Oceanic Cd/P ratio and nutrient utilization in the glacial Southern Ocean, *Nature*, *405*, 305–310.

Etheridge, D. M., L. P. Steele, R. L. Langenfelds, R. J. Francey, J.-M. Barnola, and V. I. Morgan (1996), Natural and anthropogenic changes in atmospheric CO_2 over the last 1000 years from air in Antarctic ice and firn, *J. Geophys. Res.*, *101*, 4115–4128.

Fairbanks, R. G. (1989), A 17,000-year glacio-eustatic sea level record: Influence of glacial melting rates on the Younger Dryas event and deep-ocean circulation, *Nature*, *342*, 637–642.

Fichefet, T., E. Driesschaert, H. Goosse, P. Huybrechts, I. Janssens, A. Mouchet, and G. Munhoven (2006), Modelling the evolution of climate and sea level during the third millennium (MILMO), *Final Rep. EV/09*, Belg. Sci. Policy, Brussels. (Available at http://www.belspo.be/belspo/home/publ/pub_ostc/EV/rappEV09_en.pdf)

Flores-Diaz, A. (1986), *Tlapacoya: 35,000 años de historia del Lago de Chalco*, pp. 109–156, Inst. de Antropol. e Hist., Mexico City.

Garcia, H. E., R. A. Locarnini, T. P. Boyer, and J. I. Antonov (2006), *World Ocean Atlas 2005*, vol. 4, *Nutrients (Phosphate, Nitrate, Silicate)*, edited by S. Levitus, *NOAA Atlas NESDIS*, vol. 64, NOAA, Silver Spring, Md.

Gasse, F., and E. Van Campo (1994), Abrupt post-glacial climate events in west Asia and North Africa monsoon domains, *Earth Planet. Sci. Lett.*, *126*, 435–456.

Gasse, F., R. Tehet, A. Durand, E. Gilbert, and J. C. Fontes (1990), The arid-humid transition in the Sahara and the Sahel during the last deglaciation, *Nature*, *346*, 141–146.

Gersonde, R., X. Crosta, A. Abelmann, and L. Armand (2005), Sea-surface temperature and sea ice distribution of the Southern Ocean at the EPILOG Last Glacial Maximum—A

circum-Antarctic view based on siliceous microfossil records, *Quat. Sci. Rev.*, *24*, 869–896.

Gherardi, J. M., L. Labeyrie, J. F. McManus, R. Francois, L. C. Skinner, and E. Cortijo (2005), Evidence from the northeastern Atlantic basin for variability in the rate of the meridional overturning circulation through the last deglaciation, *Earth Planet. Sci. Lett.*, *240*, 710–723.

Goosse, H., and T. Fichefet (1999), Importance of ice-ocean interactions for the global ocean circulation: A model study, *J. Geophys. Res.*, *104*, 23,337–23,355.

Goosse, H., E. Deleersnijder, T. Fichefet, and M. H. England (1999), Sensitivity of a global coupled ocean-sea ice model to the parameterization of vertical mixing, *J. Geophys. Res.*, *104*, 13,681–13,695.

Guilderson, T. P., R. G. Fairbanks, and J. L. Rubenstone (2001), Tropical Atlantic coral oxygen isotopes: Glacial-interglacial sea surface temperatures and climate change, *Mar. Geol.*, *172*, 75–89.

Haarsma, R., E. Campos, W. Hazeleger, and C. Severijns (2008), Influence of the meridional overturning circulation on tropical Atlantic climate and variability, *J. Clim*, in press.

Harada, N., N. Ahagon, T. Sakamoto, M. Uchida, M. Ikehara, and Y. Shibata (2006), Rapid fluctuation of alkenone temperature in the southwestern Okhotsk Sea during the past 120 kyr, *Global Planet. Change*, *53*, 29–46.

Haslett, S. K., and C. F. C. Davies (2006), Late Quaternary climate-ocean changes in western North Africa: Offshore geochemical evidence, *Trans. Inst. Br. Geogr.*, *31*, 34–52.

Haug, G. H., K. A. Hughen, D. M. Sigman, L. C. Peterson, and U. Röhl (2001), Southward migration of the Intertropical Convergence Zone through the Holocene, *Science*, *293*, 1304–1308.

Heinrich, H. (1988), Origin and consequences of cyclic ice rafting in the northeast Atlantic Ocean during the past 130,000 years, *Quat. Res.*, *29*, 142–152.

Hodell, D. A., J. H. Curtis, G. A. Jones, A. Higuera-Gundy, M. Brenner, M. W. Binford, and K. T. Dorsey (1991), Reconstruction of Caribbean climate change over the past 10,500 years, *Nature*, *352*, 790–793.

Houghton, R. A. (1999), The annual net flux of carbon to the atmosphere from changes in land use 1850–1990, *Tellus, Ser. B*, *51*, 298–313.

Hughen, K. A., J. T. Overpeck, L. C. Peterson, and S. Trumbore (1996), Rapid climate changes in the tropical Atlantic region during the last deglaciation, *Nature*, *380*, 51–54.

Hughen, K. A., T. L. Eglinton, L. Xu, and M. Makou (2004), Abrupt tropical vegetation response to rapid climate changes, *Science*, *304*, 1955–1959.

Indermühle, A., et al. (1999), Holocene carbon cycle dynamics based on CO_2 trapped in ice at Taylor Dome, Antarctica, *Nature*, *398*, 121–126.

Indermühle, A., E. Monnin, B. Stauffer, T. F. Stocker, and M. Wahlen (2000), Atmospheric CO_2 concentration from 60 to 20 kyr BP from the Taylor Dome ice core, Antarctica, *Geophys. Res. Lett.*, *27*, 735–738.

Intergovernmental Panel on Climate Change (2001), *Climate Change 2001: The Scientific Basis*, edited by J. T. Houghton et al., Cambridge Univ. Press, Cambridge, U. K.

Ivanochko, T. S., R. S. Ganeshram, G.-J. A. Brummer, G. Ganssen, S. J. A. Jung, S. G. Moreton, and D. Kroon (2005), Variations in tropical convection as an amplifier of global climate change at the millennial scale, *Earth Planet. Sci. Lett.*, *235*, 302–314.

Janowiak, J. E., and P. Xie (1999), CAMS_OPI: A global satellite-rain gauge merged product for real-time precipitation monitoring applications, *J. Clim.*, *12*, 3335–3342.

Johnson, T. C., E. T. Brown, J. McManus, S. Barry, P. Barker, and F. Gasse (2002), A high-resolution paleoclimate record spanning the past 25,000 years in southern East Africa, *Science*, *296*, 113–114.

Joos, F., S. Gerber, I. C. Prentice, B. L. Otto-Bliesner, and P. J. Valdes (2004), Transient simulations of Holocene atmospheric carbon dioxide and terrestrial carbon since the Last Glacial Maximum, *Global Biogeochem. Cycles*, *18*, GB2002, doi:10.1029/2003GB002156.

Justino, F. (2004), The influence of boundary conditions on the Last Glacial Maximum, Ph.D. thesis, Leibniz Inst. für Meereswiss. an der Christian-Albrechts-Univ. zu Kiel, Kiel, Germany.

Justino, F., A. Timmermann, U. Merkel, and E. P. Souza (2005), Synoptic reorganization of atmospheric flow during the Last Glacial Maximum, *J. Clim.*, *18*, 2826–2846.

Keeling, C. D., J. F. S. Chine, and T. P. Whorf (1996), Increased activity of northern vegetation inferred from atmospheric CO_2 measurements, *Nature*, *382*, 146–149.

Kienast, M., S. Steinke, K. Stattegger, and S. E. Calvert (2001), Synchronous tropical south China Sea SST change and Greenland warming during deglaciation, *Science*, *291*, 2132–2134.

Kienast, M., S. S. Kienast, S. E. Calvert, T. I. Eglinton, G. Mollenhauer, R. Francois, and A. Mix (2006), Eastern Pacific cooling and Atlantic overturning circulation during the last deglaciation, *Nature*, *443*, 846–849.

Knutti, R., J. Flückiger, T. F. Stocker, and A. Timmermann (2004), Strong hemispheric coupling of glacial climate through continental freshwater discharge and ocean circulation, *Nature*, *430*, 851–856.

Kohfeld, K. C., C. Le Quere, S. Harrison, and R. Anderson (2005), Role of marine biology in glacial-interglacial CO_2 cycles, *Science*, *308*, 74–78.

Köhler, P., F. Joos, S. Gerber, and R. Knutti (2005), Simulated changes in vegetation distribution, land carbon storage, and atmospheric CO_2 in response to a collapse of the North Atlantic thermohaline circulation, *Clim. Dyn.*, *25*, 689–708.

Koutavas, A., J. Lynch-Stieglitz, T. M. Marchitto, and J. P. Sachs (2002), El Niño-like pattern in ice age tropical Pacific sea surface temperature, *Science*, *297*, 226–230.

Krebs, U., and A. Timmermann (2007), Tropical air-sea interactions accelerate the recovery of the Atlantic meridional overturning circulation after a major shutdown, *J. Clim.*, *20*, 4940–4956.

Kucera, M., et al. (2005), Reconstruction of sea-surface temperatures from assemblages of planktonic foraminifera: Multi-technique approach based on geographically constrained calibration data sets and its application to glacial Atlantic and Pacific Oceans, *Quat. Sci. Rev.*, *24*, 951–998.

Lamb, H. F., C. R. Bates, P. V. Coombes, M. H. Marshall, M. Umer, S. J. Davies, and E. Dejen (2007), Late Pleistocene desiccation of Lake Tana, source of the Blue Nile, *Quat. Sci. Rev.*, *26*, 287–299.

Lambeck, K., M. T. Esat, and E.-K. Potter (2002), Links between climate and sea level for the past three million years, *Nature*, *419*, 199–206.

Lea, D. W., D. K. Pak, L. C. Peterson, and K. A. Hughen (2003), Synchroneity of tropical and high-latitude Atlantic temperatures over the last glacial termination, *Science*, *301*, 1361–1364.

Lim, G. H., J. R. Holton, and J. M. Wallace (1991), The structure of the ageostrophic wind field in baroclinic waves, *J. Atmos. Sci.*, *48*, 1733–1745.

Lin, H.-L., C.-T. Lai, H.-C. Ting, L. Wang, M. Sarnthein, and J.-J. Hung (1999), Late Pleistocene nutrients and sea surface productivity in the South China Sea: A record of teleconnections with Northern Hemisphere events, *Mar. Geol.*, *156*, 197–210.

Little, M. G., R. R. Schneider, D. Kroon, B. Price, T. Bickert, and G. Wefer (1997), Rapid palaeoceanographic changes in the Benguela upwelling system for the last 160,000 years as indicated by abundances of planktonic foraminifera, *Palaeogeogr. Palaeoclimatol. Palaeoecol.*, *130*, 135–161.

Maley, J., and P. Brenac (1998), Vegetation dynamics, palaeoenvironments and climatic changes in the forests of western Cameroon during the last 28,000 years B.P., *Rev. Palaeobot. Palynol.*, *99*, 157–187.

Marchal, O., T. F. Stocker, and F. Joos (1998), Impact of oceanic reorganizations on the ocean carbon cycle and atmospheric carbon dioxide content, *Paleoceanography*, *13*, 225–244.

Marchal, O., T. F. Stocker, F. Joos, A. Indermühle, T. Blunier, and J. Tschumi (1999), Modelling the concentration of atmospheric CO_2 during the Younger Dryas climate event, *Clim. Dyn.*, *15*, 341–354.

Marshall, S. J., and M. R. Koutnik (2006), Ice sheet action versus reaction: Distinguishing between Heinrich events and Dansgaard-Oeschger cycles in the North Atlantic, *Paleoceanography*, *21*, PA2021, doi:10.1029/2005PA001247.

Maslin, M. A., and S. J. Burns (2000), Reconstruction of the Amazon basin effective moisture availability over the past 14,000 years, *Science*, *290*, 2285–2287.

McManus, J. F., R. Francois, J. M. Gherardi, L. D. Keigwin, and S. Brown-Leger (2004), Collapse and rapid resumption of Atlantic meridional circulation linked to deglacial climate changes, *Nature*, *428*, 834–837.

Monnin, E., A. Indermühle, A. Dällenbach, J. Flückiger, B. Stauffer, T. F. Stocker, D. Raynaud, and J.-M. Barnola (2001), Atmospheric CO_2 concentration over the last glacial termination, *Science*, *291*, 112–114.

Mouchet, A., and L. M. Francois (1996), Sensitivity of a Global Oceanic Carbon Cycle Model to the circulation and to the fate of organic matter: Preliminary results, *Phys. Chem. Earth*, *21*, 511–516.

Myneni, R. B., S. O. Los, and G. Asrar (1995), Potential gross primary productivity of terrestrial vegetation from 1982–1990, *Geophys. Res. Lett.*, *22*, 2617–2620.

Nürnberg, D., A. Müller, and R. R. Schneider (2000), Paleo-sea surface temperature calculations in the equatorial east Atlantic from Mg/Ca ratios in planktic foraminifera: A comparison to sea surface temperature estimates from $U^{K'}_{37}$, oxygen isotopes, and foraminiferal transfer function, *Paleoceanography*, *15*, 124–134.

Opsteegh, J. D., R. J. Haarsma, F. M. Selten, and A. Kattenberg (1998), ECBILT: A dynamic alternative to mixed boundary conditions in ocean models, *Tellus, Ser. A*, *50*, 348–367.

Ortiz, J. D., J. DelViscio, W. Dean, J. D. Carriquiry, T. Marchitto, Y. Zheng, and A. van Geen (2004), Enhanced marine productivity off western North America during warm climate intervals of the past 52 k.y., *Geology*, *32*, 521–524.

Pailler, D., and E. Bard (2002), High frequency palaeoceanographic changes during the past 140,000 yr recorded by the organic matter in sediments of the Iberian Margin, *Palaeogeogr. Palaeoclimatol. Palaeoecol.*, *181*, 431–452.

Peacock, S., E. Lane, and J. M. Restrepo (2006), A possible sequence of events for the generalized glacial-interglacial cycle, *Global Biogeochem. Cycles*, *20*, GB2010, doi:10.1029/2005GB002448.

Peltier, W. R. (1994), Ice-age paleotopography, *Science*, *265*, 195–201.

Pflaumann, U., et al. (2003), Glacial North Atlantic: Sea-surface conditions reconstructed by GLAMAP 2000, *Paleoceanography*, *18*(3), 1065, doi:10.1029/2002PA000774.

Plewa, K., H. Meggers, and S. Kasten (2006), Barium in sediments off northwest Africa: A tracer for paleoproductivity or meltwater events?, *Paleoceanography*, *21*, PA2015, doi:10.1029/2005PA001136.

Prange, M., and M. Schulz (2004), A coastal upwelling seesaw in the Atlantic Ocean as a result of the closure of the Central American Seaway, *Geophys. Res. Lett.*, *31*, L17207, doi:10.1029/2004GL020073.

Rasmussen, T. L., E. Thomsen, S. R. Troelstra, A. Kuijpers, and M. A. Prins (2002), Millennial-scale glacial variability versus Holocene stability: Changes in planktic and benthic foraminifera faunas and ocean circulation in the North Atlantic during the last 60,000 years, *Mar. Micropaleontol.*, *47*, 143–176.

Renssen, H., H. Goosse, T. Fichefet, V. Brovkin, E. Driesschaert, and F. Wolk (2005), Simulating the holocene climate evolution at northern high latitudes using a coupled atmosphere-sea ice-ocean-vegetation model, *Clim. Dyn.*, *24*, 23–43.

Reynolds, R. W., and T. M. Smith (1995), A high-resolution global sea-surface temperature climatology, *J. Clim.*, *8*, 1571–1583.

Roche, D. M., T. M. Dokken, H. Goosse, H. Renssen, and S. L. Weber (2006), Climate of the last glacial maximum: Sensitivity studies and model-data comparison with the LOVECLIM coupled model, *Clim. Past Discuss.*, *2*, 1105–1153.

Rohling, E. J., A. Hayes, S. De Rijk, D. Kroon, W. J. Zacharasse, and D. Eisma (1998), Abrupt cold spells in the northwest Mediterranean, *Paleoceanography*, *13*, 316–322.

Rohling, E. J., R. Marsh, N. C. Wells, M. Siddall, and N. R. Edwards (2004), Similar meltwater contributions to glacial sea level changes from antarctic and northern ice sheets, *Nature*, *430*, 1016–1021.

Rosenthal, Y., D. W. Oppo, and B. K. Linsley (2003), The amplitude and phasing of climate change during the last deglaciation in the Sulu Sea, western equatorial Pacific, *Geophys. Res. Lett.*, *30*(8), 1428, doi:10.1029/2002GL016612.

Rühlemann, C., S. Mulitza, P. J. Müller, G. Wefer, and R. Zahn (1999), Warming of the tropical Atlantic Ocean and slowdown of thermohaline circulation during the last deglaciation, *Nature*, *402*, 511–514.

Sachs, J. P., and R. F. Anderson (2005), Increased productivity in the subantarctic ocean during Heinrich events, *Nature*, *434*, 1118–1121.

Schmittner, A. (2005), Decline of the marine ecosystem caused by a reduction in the Atlantic overturning circulation, *Nature*, *434*, 628–633.

Scholz, C. A., J. W. King, G. S. Ellis, P. K. Swart, J. C. Stager, and S. M. Colman (2003), Paleolimnology of Lake Tanganyika, East Africa, over the past 100 kyr, *J. Paleolimnol.*, *30*, 139–150.

Scholze, M., J. O. Kaplan, W. Knorr, and M. Heimann (2003a), Climate and interannual variability of the atmosphere-biosphere $^{13}CO_2$ flux, *Geophys. Res. Lett.*, *30*(2), 1097, doi:10.1029/2002GL015631.

Scholze, M., W. Knorr, and M. Heimann (2003b), Modelling terrestrial vegetation dynamics and carbon cycling for an abrupt climatic change event, *Holocene*, *13*, 327–333.

Shi, C. D., R. X. Zhu, B. P. Glass, Q. Liu, A. Zeman, and V. Suchy (2003), Climate variations since the last interglacial recorded in Czech loess, *Geophys. Res. Lett.*, *30*(11), 1562, doi:10.1029/2003GL017251.

Siddall, M., E. J. Rohling, A. Almogi-Labin, C. Hemleben, D. Meischner, I. Schmelzer, and D. A. Smeed (2003), Sea-level fluctuations during the last glacial cycle, *Nature*, *423*, 853–858.

Sowers, T., R. B. Alley, and J. Jubenville (2003), Ice core records of atmospheric N_2O covering the last 106,000 years, *Science*, *301*, 945–948.

Stager, J. C., P. A. Mayewski, and L. D. Meeker (2002), Cooling cycles, Heinrich event 1, and the desiccation of Lake Victoria, *Palaeogeogr. Palaeoclimatol. Palaeoecol.*, *183*, 169–178.

Stauffer, B., et al. (1998), Atmospheric CO_2 concentration and millennial-scale climate change during the last glacial period, *Nature*, *392*, 59–62.

Stocker, T. F. (1998), The seesaw effect, *Science*, *282*, 61–62.

Stouffer, R. J., et al. (2006), Investigating the causes of the response of the thermohaline circulation to past and future climate changes, *J. Clim.*, *19*, 1365–1387.

Street-Perrot, F. A., and R. A. Perrot (1990), Abrupt climate fluctuations in the Tropics: The influence of Atlantic Ocean circulation, *Nature*, *343*, 607–610.

Swann, G. E. A., A. W. Mackay, M. J. Leng, and F. Demory (2005), Climatic change in central Asia during MIS 3/2: A case study using biological responses from Lake Baikal, *Global Planet. Change*, *46*, 235–253.

Takahashi, T., J. Olafsson, J. G. Goddard, D. W. Chipman, and S. C. Sutherland (1993), Seasonal variation of CO_2 and nutrients in the high-latitude surface oceans: A comparative study, *Global Biogeochem. Cycles*, *7*, 843–878.

Takahashi, T., et al. (2002), Global sea-air CO_2 flux based on climatological surface ocean pCO_2 and seasonal biological and temperature effects, *Deep Sea Res., Part II*, *49*, 1601–1622.

Talley, L. D., J. Reid, and P. E. Robbins (2003), Data-based meridional overturning streamfunctions for the global ocean, *J. Clim.*, *16*, 3213–3226.

Teller, J. T., D. W. Leverington, and J. D. Mann (2002), Freshwater outbursts to the oceans from glacial Lake Agassiz and their role in climate change during the last deglaciation, *Quat. Sci. Rev.*, *21*, 879–887.

Thomas, E., L. Booth, M. Maslin, and N. J. Shackleton (1995), Northeastern Atlantic benthic foraminifera during the last 45,000 years: Changes in productivity seen from the bottom up, *Paleoceanography*, *10*, 545–562.

Thompson, L. G., E. Mosley-Thompson, M. E. Davis, P.-N. Lin, K. A. Henderson, J. Cole-Dai, J. F. Bolzan, and K. B. Liu (1995), Late glacial stage and Holocene tropical ice core records from Huascaran, Peru, *Science*, *269*, 46–50.

Thompson, L. G., et al. (1998), A 25,000-year tropical climate history from Bolivian ice cores, *Science*, *282*, 1858–1864.

Thouveny, N., J.-L. de Beaulieu, E. Bonifay, K. M. Creer, J. Guiot, M. Icole, S. J. Jouzel, M. Reille, T. Williams, and D. Williamson (1994), Climate variations in Europe over the past 140 kyr deduced from rock magnetism, *Nature*, *371*, 503–506.

Timm, O., and A. Timmermann (2007), Simulation of the last 21,000 years using accelerated transient boundary conditions, *J. Clim.*, *20*, 4377–4401.

Timmermann, A., F. Justino, F.-F. Jin, U. Krebs, and H. Goosse (2004), Surface temperature control in the North and tropical Pacific during the last glacial maximum, *Clim. Dyn.*, *23*, 353–370.

Timmermann, A., S. I. An, U. Krebs, and H. Goosse (2005a), ENSO suppression due to a weakening of the North Atlantic thermohaline circulation, *J. Clim.*, *18*, 3122–3139.

Timmermann, A., U. Krebs, F. Justino, H. Goosse, and T. Ivanochko (2005b), Mechanisms for millennial-scale global synchronization during the last glacial period, *Paleoceanography*, *20*, PA4008, doi:10.1029/2004PA001090.

Timmermann, A., et al. (2007), The influence of shutdown of the Atlantic meridional overturning circulation on ENSO, *J. Clim.*, *19*, 4899–4919.

Turney, C. S. M., A. P. Kershaw, S. C. Clemens, N. Branch, P. T. Moss, and L. K. Fifield (2004), Millennial and orbital variations of El Niño/Southern Oscillation and high-latitude climate in the last glacial period, *Nature*, *428*, 306–310.

VanDerHammen, T., and H. Hooghiemstra (1995), The El Abra stadial, a Younger Dryas equivalent in Colombia, *Quat. Sci. Rev.*, *14*, 841–851.

Vidal, L., L. Labeyrie, E. Cortijo, M. Arnold, J. C. Duplessy, E. Michel, S. Becque, and T. C. E. vanWeering (1997), Evidence for changes in the North Atlantic Deep Water linked to meltwater surges during the Heinrich events, *Earth Planet. Sci. Lett.*, *146*, 13–27.

Vink, A., C. Rühlemann, K. A. F. Zonneveld, and S. Mulitza (2001), Shifts in the position of the North Equatorial Current and rapid productivity changes in the western tropical Atlantic during the last glacial, *Paleoceanography*, *16*, 479–490.

Visser, K., R. Thunell, and L. Stott (2003), Magnitude and timing of temperature change in the Indo-Pacific warm pool during deglaciation, *Nature*, *421*, 152–155.

Wang, X., A. S. Auler, R. L. Edwards, H. Cheng, P. S. Cristalli, P. Smart, D. A. Richards, and C.-C. Shen (2004), Wet periods in northeastern Brazil over the past 210 kyr linked to distant climate anomalies, *Nature*, *432*, 740–743.

Wang, X., A. S. Auler, R. L. Edwards, H. Cheng, E. Ito, and M. Solheid (2006), Interhemispheric anti-phasing of rainfall during the

last glacial period, *Quat. Sci. Rev.*, *25*, 3391–3403.

Wang, Y. J., H. Cheng, R. L. Edwards, Z. S. An, J. Y. Wu, C. C. Shen, and J. A. Dorale (2001), A high-resolution absolute-dated late Pleistocene monsoon record from Hulu Cave, China, *Science*, *294*, 2345–2348.

Watts, W. A., J. R. M. Allen, and B. Huntley (1996), Vegetation history and paleoclimate of the last glacial period at Lago grande di Monticchio, southern Italy, *Quat. Sci. Rev.*, *15*, 133–153.

Weinelt, M., A. Rosell-Mel, U. Pflaumann, M. Sarnthein, and T. Kiefer (2003), Zur Rolle der Produktivität im Nordostatlantik bei abrupten Klimanderungen in den letzten 80,000 Jahren (The role of productivity in the northeast Atlantic on abrupt climate change over the last 80,000 years), *Z. Dtsch. Geol. Ges.*, *154*(1), 47–66.

Zhang, R., and T. L. Delworth (2005), Simulated tropical response to a substantial weakening of the Atlantic thermohaline circulation, *J. Clim.*, *18*, 1853–1860.

L. Menviel, Department of Oceanography, University of Hawai'i at Manoa, 1000 Pope Road, Honolulu, HI 96822, USA. (menviel@hawaii.edu)

A. Mouchet, Département Astrophysique, Géophysique et Océanographie, Université de Liège, B-4000 Liège, Belgium.

O. Timm and A. Timmermann, International Pacific Research Center, SOEST, University of Hawai'i at Manoa, Honolulu, HI 96822, USA.